### Title

Cell numbers, cell ratios, and developmental plasticity in the rod pathway of the mouse retina




### Journal

Journal of Anatomy, 243(2)

### ISSN

0021-8782



### Authors

Keeley, Patrick W
Patel, Shivam S
Reese, Benjamin E



### Publication Date

2023-08-01

### DOI

10.1111/joa.13653

Received: 11 January 2022 | Revised: 7 February 2022 | Accepted: 28 February 2022

DOI: 10.1111/joa.13653

Journal of Anatomy ANATOMICAL SOCIETY WILEY

REVIEW ARTICLE

# Cell numbers, cell ratios, and developmental plasticity in the rod pathway of the mouse retina

Patrick W. Keeley[1] | Shivam S. Patel[1] | Benjamin E. Reese[1,2]

[1]Neuroscience Research Institute, University of California, Santa Barbara, Santa Barbara, California, USA

[2]Department of Psychological & Brain Sciences, University of California, Santa Barbara, Santa Barbara, California, USA

**Correspondence**
Patrick W. Keeley, Neuroscience Research Institute, University of California, Santa Barbara, Santa Barbara, CA 93106-5060, USA.
Email: pwkeeley@ucsb.edu

**Funding information**
This research was supported by grants from the NIH (EY-019968; OD-010610).

## Abstract

The precise specification of cellular fate is thought to ensure the production of the correct number of neurons within a population. Programmed cell death may be an additional mechanism controlling cell number, believed to refine the proper ratio of pre- to post-synaptic neurons for a given species. Here, we consider the size of three different neuronal populations in the rod pathway of the mouse retina: rod photoreceptors, rod bipolar cells, and AII amacrine cells. Across a collection of 28 different strains of mice, large variation in the numbers of all three cell types is present. The variation in their numbers is not correlated, so that the ratio of rods to rod bipolar cells, as well as rod bipolar cells to AII amacrine cells, varies as well. Establishing connectivity between such variable pre- and post-synaptic populations relies upon plasticity that modulates process outgrowth and morphological differentiation, which we explore experimentally for both rod bipolar and AII amacrine cells in a mouse retina with elevated numbers of each cell type. While both rod bipolar dendritic and axonal arbors, along with AII lobular arbors, modulate their areal size in relation to local homotypic cell densities, the dendritic appendages of the AII amacrine cells do not. Rather, these processes exhibit a different form of plasticity, regulating the branching density of their overlapping arbors. Each form of plasticity should ensure uniformity in retinal coverage in the presence of the independent specification of afferent and target cell number.

**KEYWORDS**
amacrine cell, Bax, coverage factor, recombinant inbred strain, rod bipolar cell, rod photoreceptor

## 1 | INTRODUCTION

The anatomical organization of the central nervous system is defined by its cytoarchitecture, wherein the various types of neurons are regionally distributed. Distinct cell types are each characteristically interconnected to permit neuronal processing that underlies the functioning of the nervous system, with species-typical variation in the numbers of different types of neurons yielding much of the variation in overall brain structure observed. Indeed, precision in the mechanisms guiding neuronal fate assignment during development is believed to be critical for establishing the correct numbers of neurons in their proper ratios (Cepko et al., 1996). Others investigating programmed cell death during development regard the natural elimination of a proportion of neurons in a population to ensure the establishment of correct species-specific ratios of afferent to target neurons (Buss et al., 2006), enabling efficient functioning of the nervous system suited to each species.

We have been examining the precision by which neuronal number is specified, using the mouse retina as a model system. The layered organization of the retina lends itself to such an analysis, as it can be dissected and then sampled in its entirety, imaging through its depth without the

need for sectioning and associated correction factors. By using inbred strains of mice, one can in principle eliminate genetic contributions to understand the extent to which neuronal number in a population varies, where that variation should arise from remaining environmental factors or from technical constraints and sampling protocols that ultimately limit the resolution of absolute number. We were initially drawn to this issue as we observed apparent quantitative differences in the cytoarchitecture of the retina in two different inbred strains of mice, the C57BL/6J (B6/J) and A/J strains (Figure 1a,b), wherein both cellular and synaptic regions are larger in the former strain. Perhaps such differences simply indicate a difference in the developmental processes stipulating overall cell number while still maintaining species-typical ratios of afferent to target neurons. Our first analysis of this, comparing the relative numbers of cone photoreceptors and horizontal cells (a retinal interneuron innervated by the cones), found nearly twice as many of each cell type in the B6/J strain, yet maintaining an ~11:1 ratio of cones to horizontal cells in both strains (Reese et al., 2005), suggesting that, while the specification of absolute number might be malleable, the ratio of pre- to post-synaptic cell types may be conserved.

To examine the generality of this result, we took advantage of a panel of 26 recombinant inbred (RI) strains of mice derived from these same two parental strains, in which each of their genomes is a unique homozygous mosaic of the genetic haplotypes of the two inbred parental genomes (Williams et al., 2001). By quantifying both cone photoreceptor and horizontal cell number across the entire strain-set, we found conspicuous and graded variation in cell number across the strains (Whitney, Raven, Ciobanu, et al., 2011, Whitney, Raven, Lu, et al., 2011), but that the variation in cell number exhibited a meager correlation between the two cell types (Reese et al., 2011). Those results called into question the notion that the precise regulation of cell number ensures the establishment of a "correct" ratio of afferent to target cells.

Unlike many other retinal cell types, the population of horizontal cells does not undergo programmed cell death during development (Edqvist et al., 2008; Mayordomo, 2001; Raven et al., 2005). As interneurons, the horizontal cells provide feedback inhibition to the cones rather than transmit information radially through the retina, and are also innervated by the rod photoreceptors. We consequently wanted to revisit this issue more extensively using the radial organization of the rod pathway in the retina, where rod photoreceptors innervate a population of rod bipolar cells, and where those rod bipolar cells in turn innervate a tertiary neuron in the rod pathway, the AII amacrine cells. Those amacrine cells then relay ON versus OFF signaling through parallel cone bipolar cell types to the output neurons of the retina, the retinal ganglion cells (RGCs; Demb & Singer, 2012; Marc et al., 2014; Strettoi et al., 1992). Here, we focus on the first three cell types in this pathway, by examining the relationships between the numbers of rods, rod bipolar cells, and AII amacrine cells.

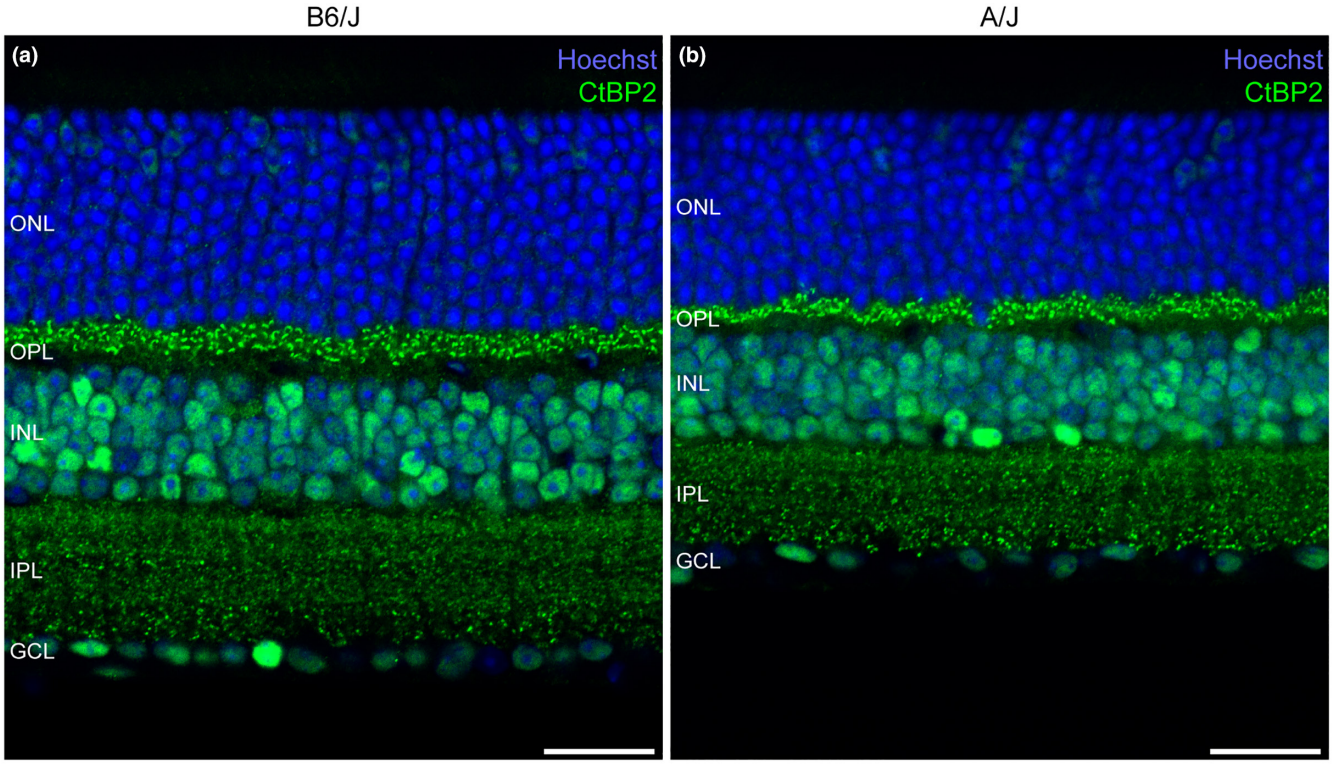


**FIGURE 1** Radial sections labeled to reveal the synaptic (CtBP2 immunolabeling) and cellular (Hoechst-33342 nuclear stain) architecture of the retina in B6/J (a) and A/J (b) mouse retinas, taken at a mid-eccentric location. At all retinal loci, the B6/J retina is thicker than the A/J retina, and this difference is apparent in both the inner nuclear layer (INL) and outer nuclear layer (ONL) as well as both plexiform layers. Those differences in thickness reflect greater numbers of cells in the ONL and INL, and their associated processes in the outer plexiform layer and inner plexiform layer. The ganglion cell layer is not thicker, but quantification of retinal ganglion cell numbers confirms the presence of more neurons in the B6/J than A/J retina. Calibration bar = 25 μm in (a) and (b)

### 1.1 | Determining cell number

As indicated above, an attraction of counting cells in the retina is that one may sample them in a wholemount preparation. As most cell types are confined to a restricted depth within the retina, imaging the population is straightforward provided each type can be reliably identified, typically immunostaining the preparation using antibodies that recognize specific cell types. Rod and cone nuclei also have characteristic nuclear chromatin patterns that permit their discrimination (Carter-Dawson & LaVail, 1979; Hughes et al., 2017). Rod photoreceptors, however, present a unique challenge, for they are stacked upon one another many times over, rendering a count of their somata time-consuming and potentially inaccurate while focusing through the entire depth of the outer nuclear layer (ONL). An option is to count their inner or outer segments, which are all packed side by side, using differential interference contrast optics to resolve them (Figure 2a). Unfortunately, those inner and outer segments of the rods and cones are not appreciably discriminated using this approach in mouse retina, but by labeling the same retinal preparations with a fluorescently tagged lectin that identifies the far rarer cone photoreceptors, one can exclude those cone counts to achieve an accurate estimate of rods only (Keeley et al., 2014).

Rod bipolar cells, situated in the outer parts of the inner nuclear layer (INL), can be labeled using antibodies to PKC, but their somata are occasionally displaced slightly in the radial axis and are frequently packed side-by-side, and the thin somal outline of a labeled cell can be hard to discriminate when it abuts many other labeled cells. Furthermore, the quality of somatic labeling is often quite variable, likely due to inadequate penetration of antibodies deep into the tissue. Methodically counting such somal profiles is in principle possible, but a faster and more consistent approach is to count instead the large radially oriented axonal stalks that pass through the INL to reach the inner depths of the inner plexiform layer (IPL) (Figure 2b). AII amacrine cells in the mouse retina, by contrast, occupy the innermost stratum of the INL, and they are commonly identified using antibodies to the transcription factor PROX1 which labels their nuclei, permitting their ready discrimination from neighboring cells (Figure 2c), aided as well by their lower densities. Their positioning at the inner margin of the INL, as well as their size, permits their discrimination from other PROX1+ cells in the outer parts of the INL.

### 1.2 | Cell number is precisely specified within any strain

Retinas vary not only in their thickness but also in their areal extent, and the latter measure is easily distorted by a host of technical issues relating to dissection, fixation, and mounting upon a slide. We have previously shown that, by sampling multiple loci upon the retina to define local densities of a particular cell type (the cholinergic amacrine cell), and then calculating an average density, that number can exhibit a degree of variability between individual retinas from the same strain of mice that is substantially lowered by multiplying that average density by total retinal area to estimate the total number per retina (Keeley et al., 2017). Table 1 illustrates this point effectively for these three cell types in the rod pathway, displaying the coefficient of variation (CoV) for average density, for retinal area, and for estimated total number, from two different strains for each cell type, in which four mice were sampled in each case. These strains were chosen for having comparable CoVs for their total estimated numbers, yet which differed in their CoVs for average density. That latter difference between the strains was likely a consequence of how much the retina was spread out upon the slide in the process of preparing the wholemount, thereby altering local cell density. By taking care to ensure the entirety of the retina is included, multiplying average density by retinal area eliminates the variation introduced in the process of preparing the retinal wholemount, in turn reducing the variance in the total cell estimate.

Somewhat remarkably, the variance within strains, across different cell types, does not correlate with the densities of the various cell types nor with the amount of retinal area sampled (Keeley et al., 2017). By computing the CoV associated with the total estimated numbers of rods, rod bipolar cells, and AII amacrine cells, respectively, for each strain, and then averaging those CoVs across all strains for each cell type, these were found to be hardly different (0.04, 0.05, and 0.05), despite their respective total numbers varying across two orders of magnitude (Keeley et al., 2014).

### 1.3 | Cell number exhibits substantial variation between strains

While we observed meager variation within any strain, large variation was observed across the strains, for each of these cell types (Figure 3). Rod photoreceptor numbers ranged from ~6,000,000 to ~8,200,000, while rod bipolar cell numbers ranged from ~202,000 to ~254,000, and AII amacrine cell numbers ranged from ~57,000 to ~87,000. The means and individual counts for each strain (color-coded) are shown in Figure 3 for each cell type, here ordered by increasing cell number. As is immediately apparent, the ordering of the strains by their rod photoreceptor number (Figure 3a) was not maintained when ordered by rod bipolar cell number (Figure 3b), and nor was the ordering of the strains by their rod bipolar cell number maintained when ordered by AII amacrine cell number (Figure 3c).

### 1.4 | Minimal co-variation between cell types is found

This change in the rank ordering of the strains does not convey the extent to which cell number across the strains may still be at least partially correlated. Figure 4, instead, plots the mean value for each strain as scatterplots comparing either the relationship between rods and rod bipolar cells (Figure 4a), or between rod bipolar cells and AII amacrine cells (Figure 4b). While there is a slight tendency for strains with greater numbers of rods to have

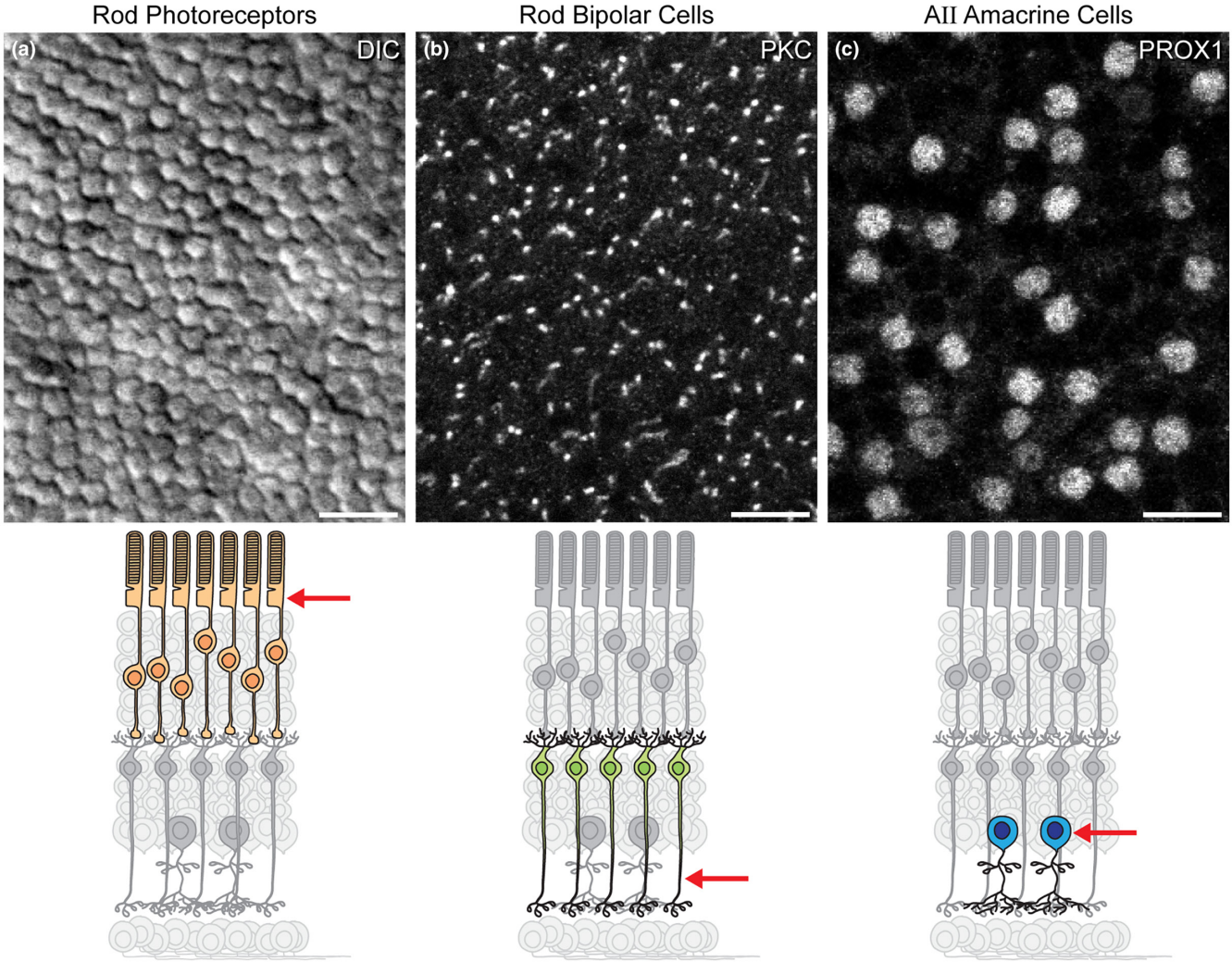


FIGURE 2 Retinal wholemount preparations showing the resolution of individual inner segments just beyond the outer limiting membrane using differential interference contrast microscopy (a), PKC immunolabeling of rod bipolar cell axons coursing through the inner plexiform layer (b), and PROX1 immunolabeling of the nuclei of AII amacrine cells at the inner margin of the inner nuclear layer (c). The approximate focal planes are illustrated beneath each micrograph. Calibration bar = 5 μm in (a); 25 μm in (b, c)

TABLE 1 Coefficient of variation (CoV) for cell density, retinal area, and estimated total number

| | Strain | CoV density | CoV retinal area | CoV Total number |
|---|---|---|---|---|
| Rod photoreceptors | AXB19 | 0.052 | 0.027 | 0.026 |
| | BXA2 | 0.033 | 0.008 | 0.027 |
| Rod bipolar cells | BXA14 | 0.078 | 0.069 | 0.050 |
| | AXB19 | 0.056 | 0.031 | 0.050 |
| AII amacrine cells | AXB6[a] | 0.096 | 0.066 | 0.038 |
| | BXA16 | 0.041 | 0.032 | 0.038 |

[a]This strain was not sampled for RBCs, and so is not indicated in Figures 3–5 (see appendix in Keeley et al., 2014).

greater numbers of rod bipolar cells, the Pearson correlation coefficient is only 0.24. The same is true when comparing rod bipolar cell numbers to AII amacrine cell numbers across the strains, yielding a correlation coefficient of 0.31, neither being statistically significant (Keeley et al., 2014). The specification of cell number for afferent and target populations is, consequently, largely independent of one another.

### 1.5 | Pre- to post-synaptic cell ratios are not preserved across strains

Such independent variation must indicate that the ratios between these pairs of cell types should not be conserved, and we can show this directly by computing those very ratios for each strain. The ratio of rods to rod bipolar cells ranged from a low of 27 to a high of 39 across these individual strains (Figure 5a), while the ratio of rod bipolar cells to AII amacrine cells ranged from 2.6 to 4.0 (Figure 5b). The latter variation did not compensate for variation in the former in order to conserve across strains a constant ratio of rod photoreceptors to AII amacrine cells, as this ratio also varied, from 87 to 126 (Figure 5c). Of course, different cell types in the mouse retina may exhibit variation in their densities as

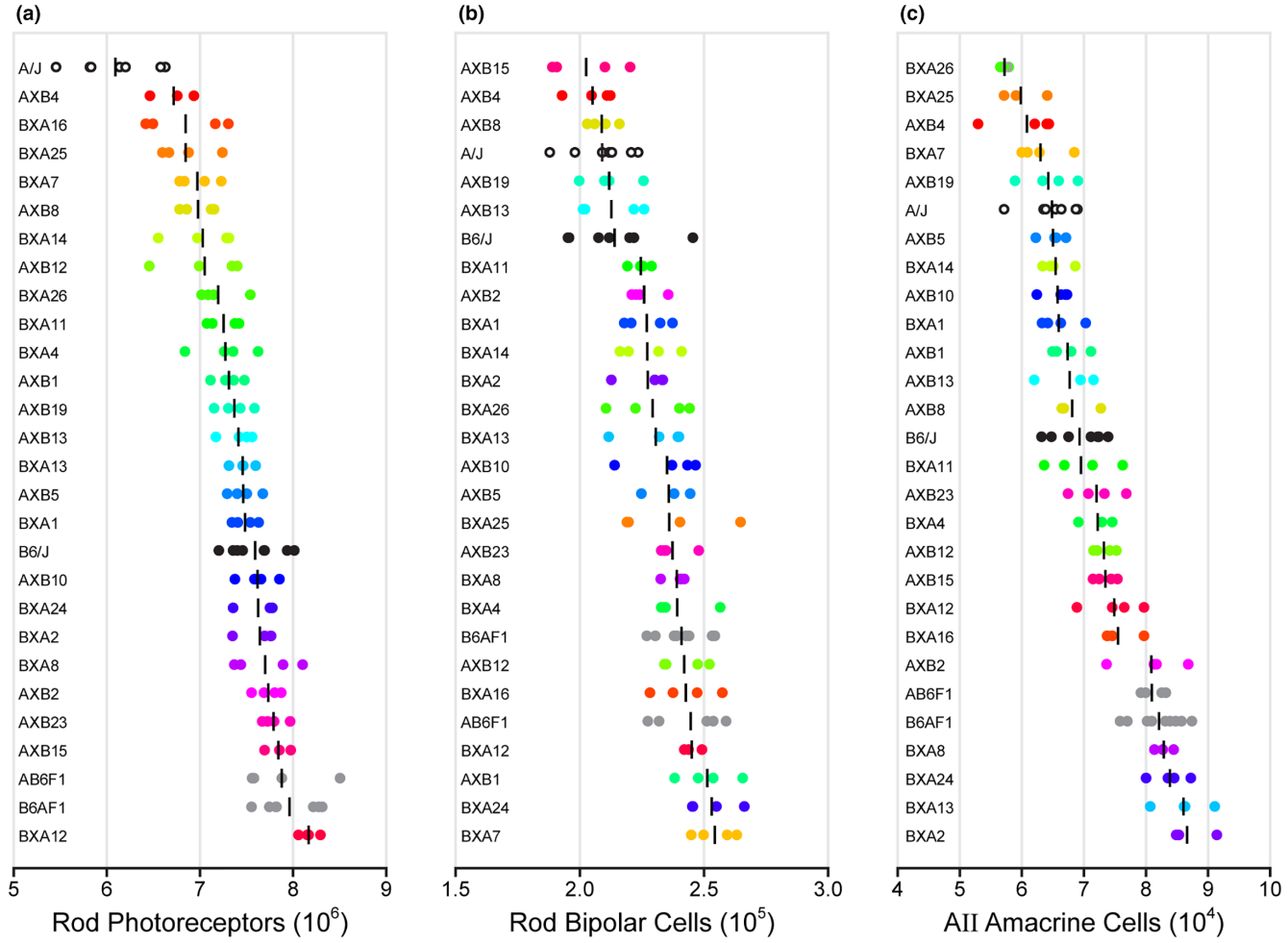


**FIGURE 3** Strain distribution patterns showing the variation in the estimated total number of rod photoreceptors (a), rod bipolar cells (b), and AII amacrine cells (c) across the set of recombinant inbred strains (colored), their parental strains (black or white), and the respective F1 crosses (grey). Strains are ranked from top to bottom in ascending order by cell number in each histogram, being color-coded to show how the strain distribution pattern changes across cell type. Strain means are indicated, with individual retinas being indicated by open or filled circles. Note that the average within-strain variation in cell number is meager relative to the large inter-strain variation, indicating that cell number is a heritable trait, while the graded distribution reveals it to be a complex trait controlled by multiple genetic variants, for each cell type. (data from the online appendix of Keeley et al., 2014)

a function of retinal eccentricity (Jeon et al., 1998) or polarity (Bleckert et al., 2014; Camerino et al., 2021; Nadal-Nicolas et al., 2020), and so these whole population ratios may conceal additional within-retinal variation in afferent-target ratios as a function of retinal locus. Regardless, the above results make clear that different strains of mice rather accurately specify the total number of each of these cell types, but their tight specification cannot be for the purpose of preserving a species-specific ratio of afferents to target cells.

## 1.6 | Morphological plasticity accommodates independent variation in cell numbers

This large and graded variation in cell number across these strains is indicative of the action of multiple causal genetic variants peppering the genomic landscape of the mouse (Keane et al., 2011; Yalcin et al., 2011), each modulating gene function or gene expression to affect various features of retinal organization including quantitative traits like cell number (Reese & Keeley, 2016). More remarkable is the plasticity by which the nervous system generates its connectivity in the presence of such variation in cell number. For instance, the variation in horizontal cell number mentioned above is inversely correlated with the size of a horizontal cell's dendritic field, thought to be mediated by homotypic interactions between neighboring cells that lead to a constant dendritic overlap (or "coverage factor") of ~6 (Reese et al., 2005), achieved when radial dendritic length approximates average intercellular distance (Szmajda et al., 2005). Within those dendritic fields, horizontal cells connect to all of the cone pedicles lying within their fields. As a consequence, the independent genetic specification of cone photoreceptor and horizontal cell numbers ultimately controls the number of cones to which a horizontal cell is connected (Reese et al., 2005). These conclusions drawn from inter-strain comparisons are borne out by studying genetic manipulations that either increase or decrease the number of horizontal cells while leaving cone density unaffected, in turn reducing or expanding the size of their

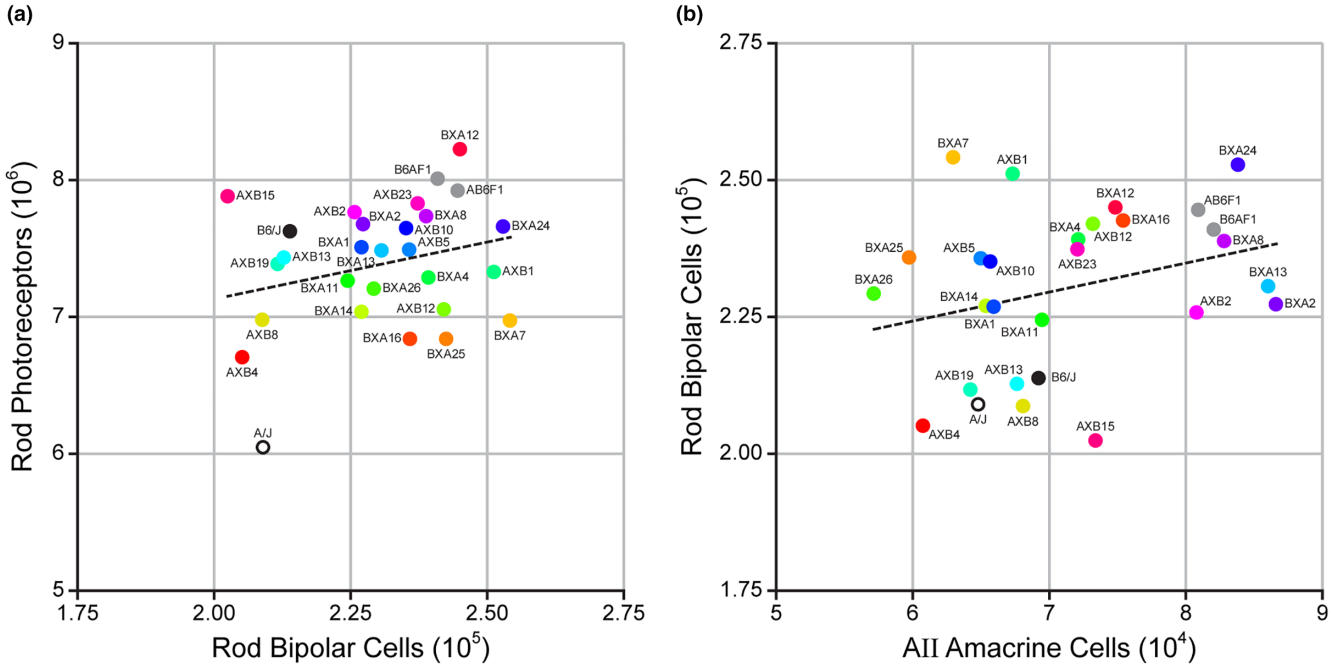


**FIGURE 4** Scatterplots derived from the data in Figure 3 showing the relationship between strain means for rod photoreceptor number and rod bipolar cell number (a), or for rod bipolar cell number and AII amacrine cell number (b). While there is a slight trend to a positive correlation in each comparison, it is not significant. Note the large variation in the number of one cell type across strains where the other hardly varies. (data from figure 2 of Keeley et al., 2014)

dendritic areas, and yielding fewer or greater numbers of cone pedicles contacted, respectively (Poché et al., 2008; Reese et al., 2011). Similar results have been obtained when considering the Type 7 cone bipolar cell, a cell type with a dendritic coverage factor of ~1 (Wässle et al., 2009): genetic manipulations that either increase or decrease the density of this cell type, while leaving cone density unaffected, yield dendritic fields that vary in size accordingly, now receiving either fewer or greater numbers of cone contacts (Lee et al., 2011). This synaptic convergence, therefore, is ultimately a byproduct of the independent specification of local presynaptic (cone) versus post-synaptic (bipolar or horizontal cell) density rather than being some species-specific trait honed over evolutionary time. Might such plasticity also characterize the behavior of the secondary and tertiary neurons in the rod pathway in the presence of such independent variation in pre- and post-synaptic cell numbers?

## 2 | MATERIALS AND METHODS

### 2.1 | Tissue collection

Mice containing a knockout *Bax* allele ($Bax^{tm1Sjk}$/J; RRID:IMSR_JAX:002994) were originally imported from The Jackson Laboratory and backcrossed for over 10 generations with B6/J mice (C57BL/6J; RRID:IMSR_JAX:000664); heterozygous mice were then crossed to produce *Bax* wildtype (WT) and *Bax* knockout (KO) littermates. Additionally, mice possessing the *Cdh1-GFP* transgenic reporter allele ($Tg[Cdh1\text{-}EGFP]^{AR201Gsat}$/Mmucd; RRID:MMRRC_011775-UCD) were obtained from the laboratory of Rachel Wong and then crossed with heterozygous *Bax* mice, so that the population of AII amacrine cells could be identified based on GFP fluorescence (Gamlin et al., 2020). The A/J and B6/J mice, their F1 crosses, and the AXB/BXA RI strain-set were used in previous analysis and have been described elsewhere (Keeley et al., 2014). All mice used in this study were considered adults, being at least 60 days of age. All procedures involving mice were done with approval from the Institutional Animal Care and Use Committee at UCSB and following the National Institutes of Health *Guide for the Care and Use of Laboratory Animals*.

For single-cell labeling, animals were euthanized with a lethal dose of sodium pentobarbital (Euthasol; 120 mg/kg) given via intraperitoneal injection. Eyes were dissected from the orbits and placed in 4% paraformaldehyde (PFA) in 0.1 M phosphate buffer (PB) for 5 min, after which the cornea, iris, and lens were removed. The eyecups remained in fixative for an additional 25 min and then transferred to PB, at which point the retinas were dissected and four relieving cuts were made to allow them to lie flat. For immunofluorescence without single-cell labeling, mice were euthanized as above, and, after ablation of the tail pinch reflex, their tissues were fixed by intracardial perfusion of 1 ml saline followed by 50 ml PFA delivered via gravity. Eyes were removed and retinas were dissected into flatmounts; these flatmounts were either processed immediately or were embedded in 5% agarose and sectioned into 200 µm-thick sections on a Pelco easySlicer. The sample used for serial block-face scanning electron microscopy was identical to the WT sample described previously (Keeley et al., 2013).

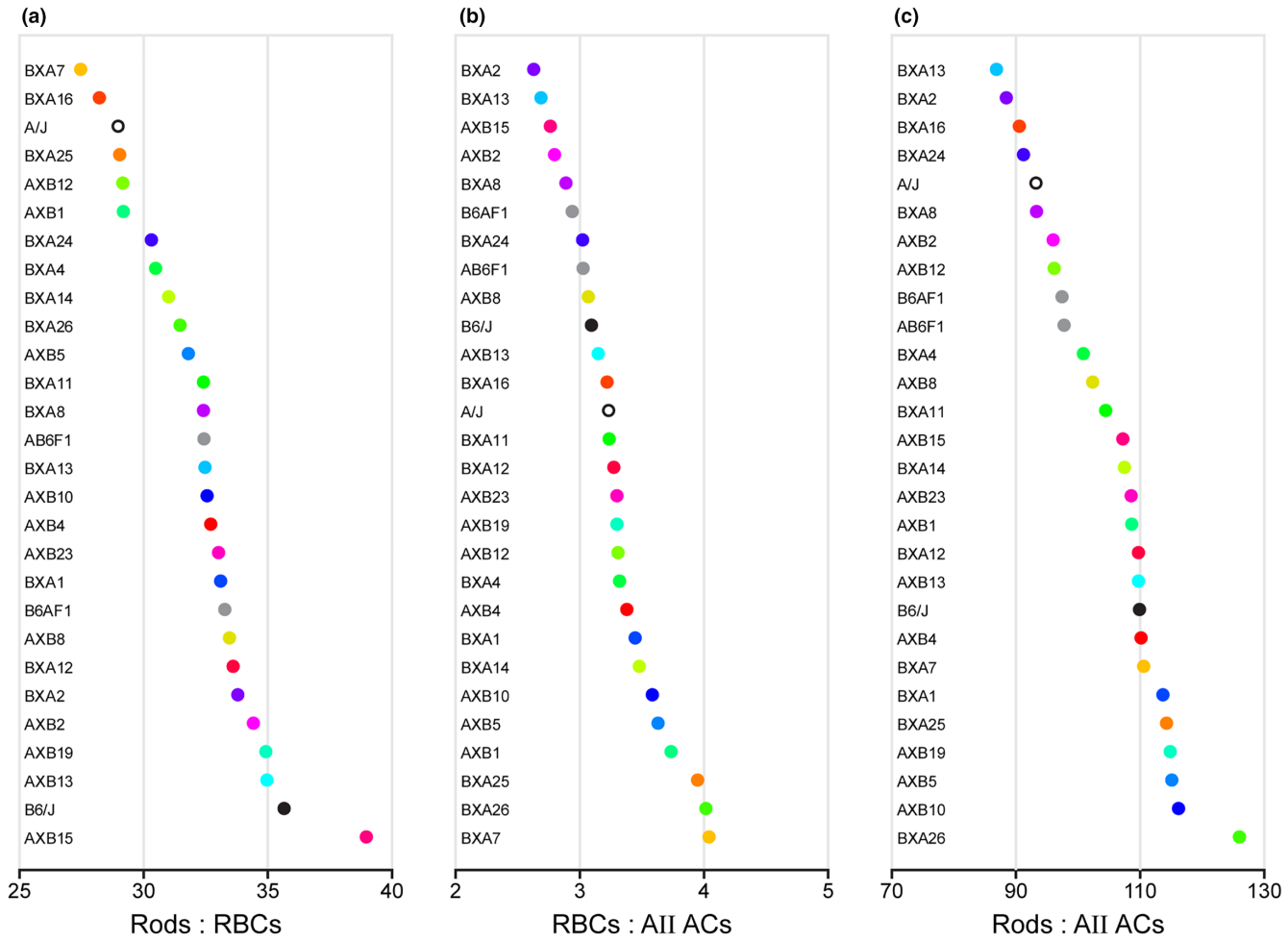


**FIGURE 5** Strain distribution patterns showing the variation in the ratio between rod photoreceptors and rod bipolar cells (a), between rod bipolar cells and AII amacrine cells (b), and between rod photoreceptors and AII amacrine cells (c), computed from the strain means in Figure 3. Strains are ordered from top to bottom by ascending ratios in each case, maintaining the same color-coding of strains established in Figure 3a. The independent variation in cell number yields variable pre- to post-synaptic ratios across the strains. Note that the variation in (b) does not compensate for the variation in (a) to render a conserved ratio of rod photoreceptors to AII amacrine cells, shown in (c). Each strain has its own unique ratios of pre- to post-synaptic cells, making clear that the precision in specifying cell number does not establish a species-specific ratio of afferent to target cells

## 2.2 | Single-cell injection

Retinas were mounted on a slide using a piece of weighing paper such that a small opening in the center allowed access to the retina, and then covered with 0.1 M PB. Retinas were then transferred to a fixed stage Nikon E600 fluorescent microscope equipped with a Burleigh micromanipulator for single-cell injection of fluorescent dyes. A glass pipette was pulled from a capillary tube to have a tip diameter of about one half a micron, filled with either the lipophilic dye DiI or the hydrophilic dye AlexaFluor568 (AF568), and guided into the retina under visual control. To label rod bipolar cells, a small crystal of DiI was deposited by passing positive current for about 10 s at either the innermost stratum of the IPL or the outermost stratum of the INL, to label dendritic or axonal arbors, respectively. To label AII amacrine cells, GFP+ somata were pierced with the pipette tip and AF568 was allowed to fill the entirety of the cell by passing negative current for about 1 min. After injection, DiI labeled retinas were post-fixed for an additional hour in 4% PFA, then imaged within 24 h; AF568 labeled retinas were subsequently processed for immunofluorescence.

## 2.3 | Immunofluorescence and microscopy

Retinal flatmounts and sections were immunolabeled using the following incubation protocol: 3 h in 5% normal donkey serum diluted in phosphate-buffered saline with 1% TritonX-100 (PBST); three 10-min rinses in PBS; three nights in primary antibodies diluted in PBST; three 10-min rinses in PBS; overnight in secondary antibodies diluted in PBST; and then three 10-min rinses in PBS. All incubations were performed with agitation at 4°C. Primary antibodies used in this study were: mouse monoclonal antibodies to C-terminal binding protein 2 (CtBP2; 1:250; RRID:AB_399431); mouse monoclonal antibodies to Protein Kinase C (PKC; 1:500; RRID:AB_568862); rabbit polyclonal antibodies

to Prospero Homeobox 1 (PROX1; 1:1000; RRID:AB_10064230); chicken polyclonal antibodies to Green Fluorescent Protein (GFP; 1:1000; RRID:AB_2534023); and rabbit polyclonal antibodies Connexin 36 (CX36; 1:500; RRID:AB_2533260). Secondary antibodies used in this study were: donkey polyclonal antibodies to mouse IgG conjugated to AlexaFluor488 (1:200; RRID:AB_2340846); donkey polyclonal antibodies to rabbit IgG conjugated to AlexaFluor647 (1:200; RRID:AB_2492288); and donkey polyclonal antibodies to chicken IgY conjugated to AlexaFluor488 (1:200; RRID:AB_2340375). The nuclear stain Hoechst-33342 (1:1000) was added to some samples along with the secondary antibodies. All samples were imaged using an Olympus Fluoview1000 laser scanning confocal microscope equipped with a 40× oil-immersion lens with a numerical aperture of 1.30, except for the retinas used to determine rod photoreceptor number, which were imaged using a Nikon FXA fluorescent microscope equipped with a 60× oil-immersion lens with a numerical aperture of 1.40.

### 2.4 | Quantification of cell number

Six *Bax* WT and six *Bax* KO mice were used to determine the number of AII amacrine cells. Retinal flatmounts were processed for PROX1 immunofluorescence and eight sample fields were taken across the retina, four central fields, and four peripheral fields, from which cellular density was determined; the average density across all eight fields was multiplied by retinal area to get an estimate of total cell number. AII amacrine cells were identified as brightly labeled large PROX1+ somata residing in the innermost layer of the INL. Three *Bax* WT and three *Bax* KO mice were used to determine the number of rod photoreceptors. Retinal flatmounts were kept flat on a glass slide with a coverslip and then soaked in a 2% PFA/2% glutaraldehyde fixative solution overnight, after which they were incubated in a 5% solution of peanut agglutinin (PNA) conjugated to AlexaFluor488 for one additional night. Retinas were rinsed and then mounted ganglion cell layer (GCL) down, and sample fields were imaged at 1 mm intervals across a square grid. At each field, all photoreceptor inner segments were counted using differential interference contrast (DIC) microscopy, then cone photoreceptors were subtracted from the counts using the fluorescent PNA signal. Average rod photoreceptor density was multiplied by retinal area to estimate total number.

### 2.5 | Morphometric analysis

All morphometrics were taken from confocal Z-stack reconstructions of single cells using a combination of ImageJ and Adobe Photoshop. For each rod bipolar cell, the axonal arbor area and dendritic field areas were determined by creating a maximum projection of each arbor, then fitting a convex polygon around its circumference. The terminal endings of each dendritic branch were labeled to determine overall number of dendritic terminals (the sites of rod spherule invagination), while the number of optical planes between the innermost and outermost terminals were used to determine the depth of the dendritic arbor. For each AII amacrine cell, the lobular field and dendritic field areas were calculated by measuring the area of the convex polygon for every optical plane that contained the arbor, and then calculating the average field area; depth of arborization was also determined from the number of these optical sections. The local density of AII amacrine cells was determined for the injected cell by counting the number of GFP+ cells in the sample field (a 0.0063 $mm^2$ square field centered on the injected cell). Branch density was determined by manual thresholding the dendritic arbor to create a binary mask, then calculating the area occupied by the branches; volumes were determined by summing these areas from each plane of the arbor. The z-stack of CX36 immunolabeling for each cell was deconvolved using ImageJ to eliminate background noise and subsequently thresholded into a binary mask. These image stacks were then overlaid with the thresholded dendritic arbor, and the total number of CX36 puncta per arbor was quantified. A CX36 punctum was counted if it persisted through several optical planes, forming a roughly spherical shape, and any part of the punctum overlapped with the dendritic arbor.

### 2.6 | Statistical analysis

All comparisons between A/J and F1 mice, and between *Bax* WT and *Bax* KO mice, were tested for statistical significance using a two-tailed Student's *t*-test, assuming equal variance. The alpha threshold for significance was set at 0.05. Individual sample fields, for cell counts, and individual labeled cells, for morphometrics, were randomized and coded so that all analyses, including thresholding, were performed blind to condition.

## 3 | RESULTS

### 3.1 | Rod bipolar cell plasticity

The dendritic arbors of single rod bipolar cells can be labeled by injecting DiI into their axon terminals, as can their axon terminals by injecting their somata (Figure 6a), targeted by virtue of their expressing the *Gustducin-GFP* reporter (Keeley & Reese, 2010), or by impaling them randomly at these respective depths within the retina, due to their heightened densities. Rod bipolar cells have a characteristic dendritic morphology, displaying a profusion of fine dendritic endings distributed across the entire thickness of the outer plexiform layer (OPL) (Figure 6b,c), the majority believed to invaginate single rod photoreceptor spherules (Anastassov et al., 2019; Keeley & Reese, 2010). As mentioned above, rod bipolar cells are frequently positioned side by side (Figure 6f), yet their dendritic fields exceed the areal domain of their somata (e.g. Figure 6b,d), reaching into the dendritic domains of neighboring cells where their processes become intermingled (Figure 6g). Those intermingled dendritic

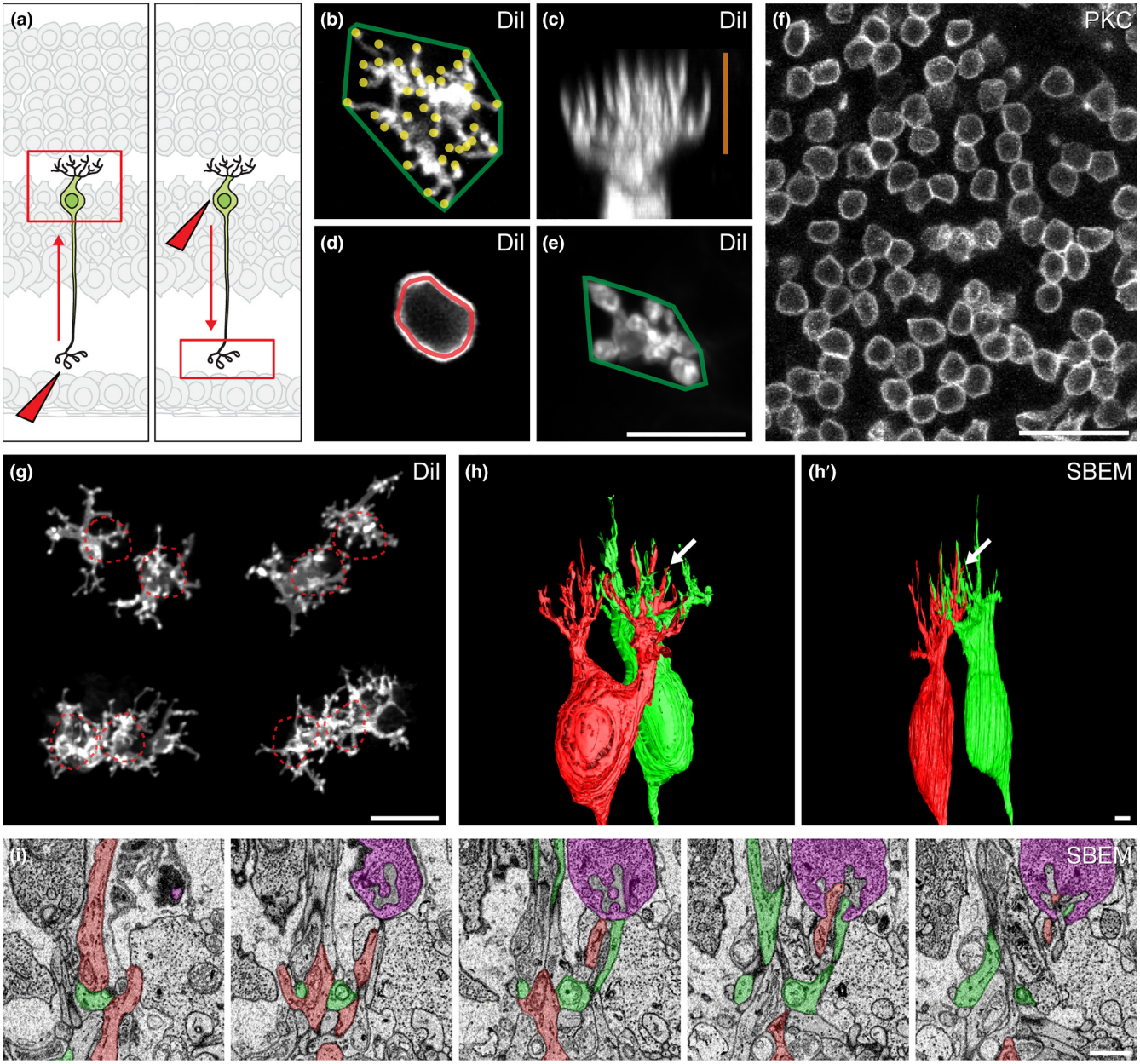


**FIGURE 6** Individual rod bipolar cells can be labeled with DiI to reveal the fine details of the dendritic or axonal arbors (a). Various morphometric features can be determined for each labeled cell, including the dendritic field area and the number of dendritic terminals (b), the depth of the outer plexiform layer (OPL) occupied by those dendritic terminals (c), the somal area (d), and the axonal arbor area in the inner plexiform layer (e). In wholemount preparations, their somata, revealed by PKC immunolabeling, are frequently packed side by side (f), and the dendritic arbors of more closely positioned neighboring cells are often, but not always, intermingled (those that cannot be discriminated with certainty are consequently excluded from the morphological analysis) (g). Reconstruction from serial block-face electron microscopy images of the OPL confirms that many of the intermingled dendritic endings from neighboring rod bipolar cells [red and green in (h), side view in (h′)] invaginate the same rod spherules [e.g. arrow in (h, h′) indicates the location of the spherule indicated in magenta in (i)]. (unpublished results from Keeley et al., 2013). Calibration bar = 10 μm in (b–e) and (g); 25 μm in (f); 1 μm in (h, i)

endings frequently converge on single spherules so that each spherule receives a single process from two neighboring rod bipolar cells (Figure 6h,i). But because multiple neighboring (often side-by-side) rod bipolar cells reach into one another's dendritic fields in order to ensure dual occupancy of single spherules, the population of spherules contacted by a rod bipolar cell is not inclusive of every spherule lying within the area of the dendritic field (Johnson et al., 2017; Tsukamoto & Omi, 2013).

Both of these features of the dendritic arbor, its areal extent and the number of dendritic terminal endings, are plastic rather than being intrinsically specified, such that the total number of those fine dendritic tips within an arbor is constrained by the local density of rod photoreceptors lying within the dendritic field, while the size of that dendritic field is itself constrained by the local density of the rod bipolar cells. To demonstrate this, we quantified the change in rod bipolar cell morphology in two sets

of comparisons. First, we compared rod bipolar cells from the A/J strain to those from the two F1 crosses, being the B6AF1 and AB6F1 (F1 hereafter) strains; we chose these strains, as the latter two have a greater number of both rod bipolar cells and rod photoreceptors (Figure 3a,b) (Keeley et al., 2014). Second, we compared cells from retinas that lack the pro-apoptotic gene *Bax* to those from WT littermates. Many cell types have elevated numbers in these *Bax* knockout (KO) retinas, including the rod bipolar cells (Simmons et al., 2019). The thickness of the ONL and OPL remains unchanged (Lee et al., 2011; Péquignot et al., 2003), however, suggesting that rod photoreceptor number is unaltered; indeed, we found that counts of rod photoreceptors do not significantly differ in the absence of *Bax* (WT: mean ± SEM = 7,625,975 ± 188,281, $n = 3$; KO: mean ± SEM = 7,913,681 ± 198,660, $n = 3$; $p = 0.353$).

In both comparisons, single labeled rod bipolar cells showed significantly reduced dendritic field areas in retinas with greater numbers of homotypic cells (Figure 7a,b). Coincident with the reduction in dendritic field area in the *Bax* KO retinas (~24%; Figure 7b), the number of dendritic terminal endings was also significantly reduced (~20%; Figure 7f); in the F1 strains, by contrast, despite the reduction in dendritic field area (Figure 7a), these rod bipolar cells had a small but significant *increase* in the number of dendritic terminals when compared to the A/J strains (Figure 7e). We attribute this to the massive increase in the rod photoreceptor population in the F1 strains relative to the A/J strain (~32%; Figure 3a), leading to an increased thickness in the OPL as it accommodates a greater number of rod spherules (Keeley et al., 2014; see also, e.g. Figure 1). Accordingly, the dendritic terminals in the F1 strains span a greater depth within the thicker OPL, by ~26% (Figure 7c). In the *Bax* KO retinas, the depth of termination is hardly, though significantly, changed (~8% decrease, Figure 7d), so that the decline in rod spherules contacted (Figure 7f) is driven mainly by the reduction in dendritic field area (Figure 7b). Others have shown exactly the reverse effect we find in the *Bax* KO, by using genetic manipulations that *reduce* rod bipolar cell density while leaving rod photoreceptor numbers unchanged: larger dendritic field areas that contact a larger number of rod spherules (Johnson et al., 2017) (Figure 7i, far right panel).

Whether the dendritic fields of rod bipolar cells are controlled directly by homotypic interactions with neighboring rod bipolar cells, or if this inverse relationship between cell density and dendritic field extent is mediated indirectly by the local constraint upon a spherule's dual occupancy, is unknown. The outgrowing dendritic terminals of rod bipolar cells in the OPL may simply extend until they confront spherules that are already occupied by a pair of dendritic terminals from two other neighboring rod bipolar cells. Their axon terminal arbors within the IPL, in comparison, have an areal extent roughly half that of the dendritic arbor, and these processes do not invade one another's territories, creating a tiling mosaic of their arbors in the innermost stratum (Young & Vaney, 1991). Like their dendritic arbors, the axonal arbors increase or decrease in areal extent when local rod bipolar cell density is reduced or enhanced, either via genetic manipulation or by comparing across strains of differing rod bipolar cell density (Figure 7g–i) (Johnson et al., 2017; Keeley et al., 2014). Within the IPL, they innervate the arboreal dendrites of AII amacrine cells, where, we might again expect, due to the independent genetic specification of their respective cell numbers, the number of rod bipolar axon terminals converging on a single AII dendritic arbor should be a product of these two independent factors controlling the densities of rod bipolar cells and of AII amacrine cells, the latter ultimately defining the areal extent of the AII amacrine cell dendritic arbors. To our surprise, AII amacrine cells do not show the same relationship between cell density and dendritic field extent.

## 3.2 | AII amacrine cell plasticity

Single AII amacrine cells can likewise be targeted for injection (Figure 8), either non-selectively by injecting somata at the inner boundary of the INL, due to their being the densest amacrine cell type positioned at the border with the IPL, or selectively by using the *Cdh1-GFP* reporter specific to AII amacrine cells (Figure 8b). Unlike the *Gustducin-GFP* reporter, which is incompletely expressed in the rod bipolar cell population, this AII-specific reporter provides excellent fidelity within the population of AII cells. A consequent attraction of the latter approach is that the areal size of the processes of an injected cell can be related to the local density of AII amacrine cells in the same field (Figure 8b), enabling a determination of the coverage factor for each cell. These cells in the mouse retina have a characteristic multi-stratified narrow-field dendritic arbor that arises from a large dendritic stalk reaching into the IPL, giving off two sets of processes, the "lobular appendages" that terminate in the outer (OFF) stratum of the IPL (Figure 8c,d), where they exchange synaptic contacts with various OFF cone bipolar cells, primarily with the Type 2 cone bipolar cells (Graydon et al., 2018; Tsukamoto & Omi, 2017), and the "arboreal dendrites" that arborize in the inner (ON) stratum of the IPL, being the target of those rod bipolar axon terminals (Famiglietti & Kolb, 1975) (Figure 8c,e).

The lobular appendages extend laterally to the tips of neighboring lobular terminal fields (Figure 8b), tiling the retina (Gamlin et al., 2020; Vaney, 1985; Vaney et al., 1991). When AII amacrine cell number is increased, by about one-third in the *Bax* KO retina (WT: mean ± SEM = 60,086 ± 1913, $n = 6$; KO: mean ± SEM = 80,563 ± 2713, $n = 6$; $p < 0.001$), the higher densities of AII amacrine cells constrain the extent of their lobular outgrowth as expected, exhibiting significantly smaller field areas in the *Bax* KO retina (Figure 9a). That reduction in lobular field area, consequently, scales precisely with the increase in local density, so that if the coverage factor (lobular field area × cell density within the sampled field) is calculated for each of these 122 individual cells, it is similar in the two conditions, being close to 1.0 (Figure 9b).

The arboreal dendrites of AII amacrine cells, by contrast, overlap with homotypic neighbors (Figure 8b), sharing gap-junctional contacts with one another along with ON cone bipolar cells, as well as receiving rod bipolar cell innervation (Marc et al., 2014; Mills et al., 2001). In the presence of increased densities of AII amacrine cells in the *Bax* KO retina, dendritic field areas do not scale down in

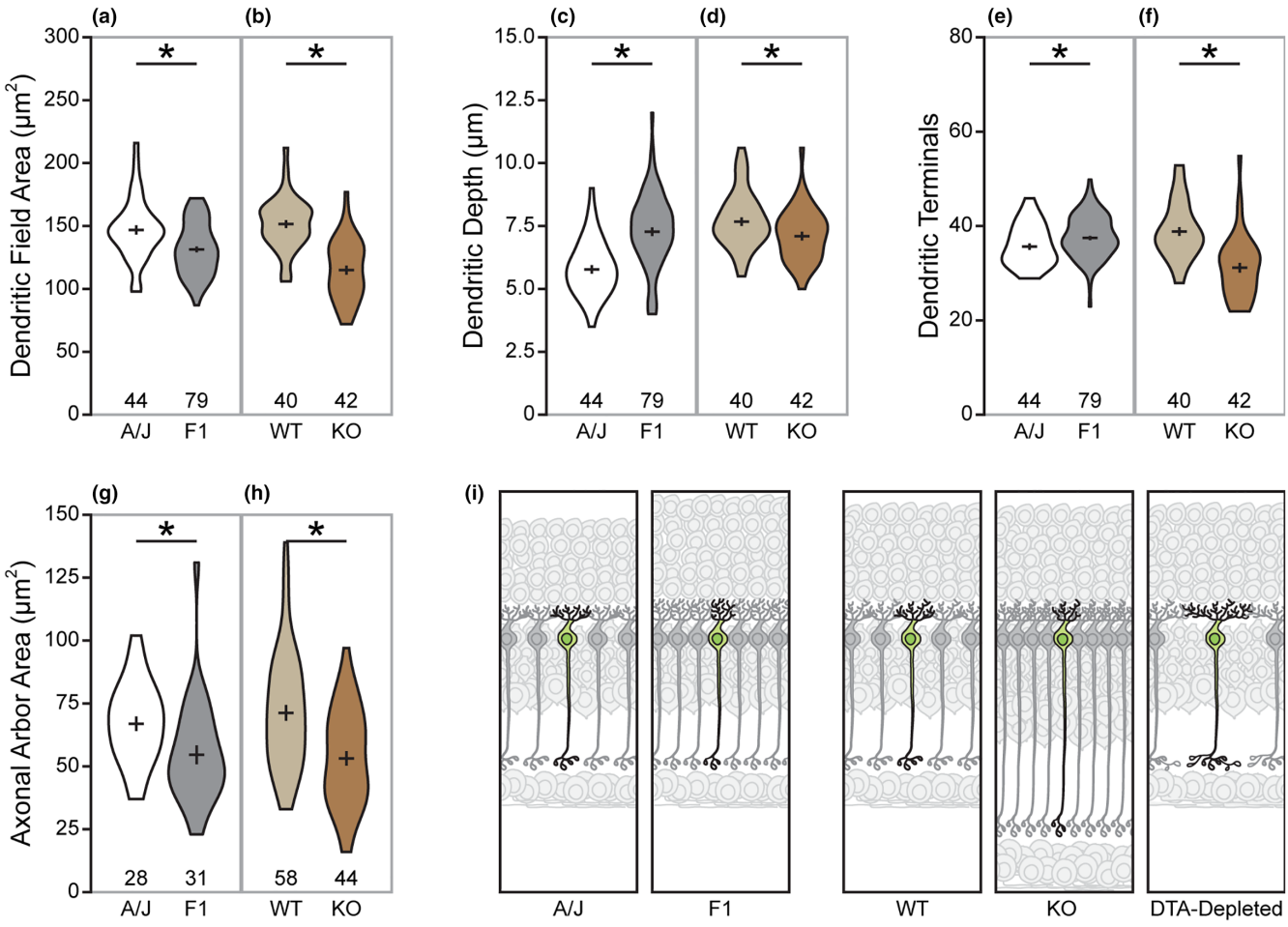


**FIGURE 7** Rod bipolar cell number is greater in the B6AF1 relative to the A/J retina and in the *Bax* KO relative to its littermate control *Bax* WT retina, and as a consequence, the dendritic field areas of rod bipolar cells are significantly smaller in the B6AF1 strain when compared to the A/J strain (a; $p < 0.001$) and in the *Bax* KO mouse relative to its *Bax* WT control (b; $p < 0.001$). Rod photoreceptor number is also greater in the B6AF1 than in the A/J retina, permitting an examination of the effect of increasing afferent number when dendritic field size is reduced. Dendritic arbors extend their terminal endings to innervate spherules distributed across a thicker outer plexiform layer in the B6AF1 relative to A/J retinas (c; $p < 0.001$); in comparison, there is only a slight difference in the depth distribution of dendritic endings in the *Bax* KO versus WT retinas (d; $p = 0.017$), where afferent density is not significantly different. The number of dendritic terminals per rod bipolar cell is slightly greater in the B6AF1 retina, despite a smaller dendritic field area, relative to A/J (e; $p = 0.032$), due to the increased density of rods, whereas the number of terminals is decreased in the *Bax* KO retina (f; $p < 0.001$), as expected from smaller dendritic fields amidst an unchanging number of rods. Axonal arbor area is reduced in both the B6AF1 (g; $p < 0.001$) and *Bax* KO retinas (h; $p < 0.001$), due to their tiling behavior in the presence of greater densities in both cases. (All data for the strain comparisons from figure 4 of Keeley et al., 2014). Rod bipolar cells, therefore, modulate the size of their dendritic arbors according to local homotypic density, while the number of dendritic endings is controlled by the density of rod spherules lying within that dendritic field area, summarized here for the comparisons between the two strains that differ in both rod bipolar cell number and in rod photoreceptor number, and for the comparisons where only rod bipolar cell number is modulated, either increased or decreased in density (i). For all measurements of individually labeled cells, here and in subsequent figures, sample distributions are illustrated using violin plots, with means and standard errors indicated by the cross within the plot. *n* = the number of cells analyzed in each group; *indicates statistically significant result

proportion to that increase in density, unlike their lobular field areas (Figure 9c). These results are consistent with those from rabbit retina where the lobular appendages maintain an average coverage factor close to 1 across the retina despite large variation in cell density while the arboreal dendrites vary in their degree of dendritic overlap, yielding coverage factors varying from ~2 to ~10 (Vaney et al., 1991). While the *Bax* KO and littermate control retinas do not exhibit such a large difference, the dendritic coverage factor increases in the *Bax* KO retina (Figure 9d).

These results make clear that, unlike the two sets of processes of the rod bipolar cell, one of the two sets of processes of the AII amacrine cell does not have its areal growth constrained by homotypic neighbors. While we could not label axonal and dendritic arbors in the same set of rod bipolar cells (Figure 6a), the proportionately comparable reduction in both areal domains confirms that they scale identically (compare Figure 7a,b, with 7g,h). In the case of the AII amacrine cells, we can assess this directly for individual cells, computing the ratio of the dendritic field area to the lobular

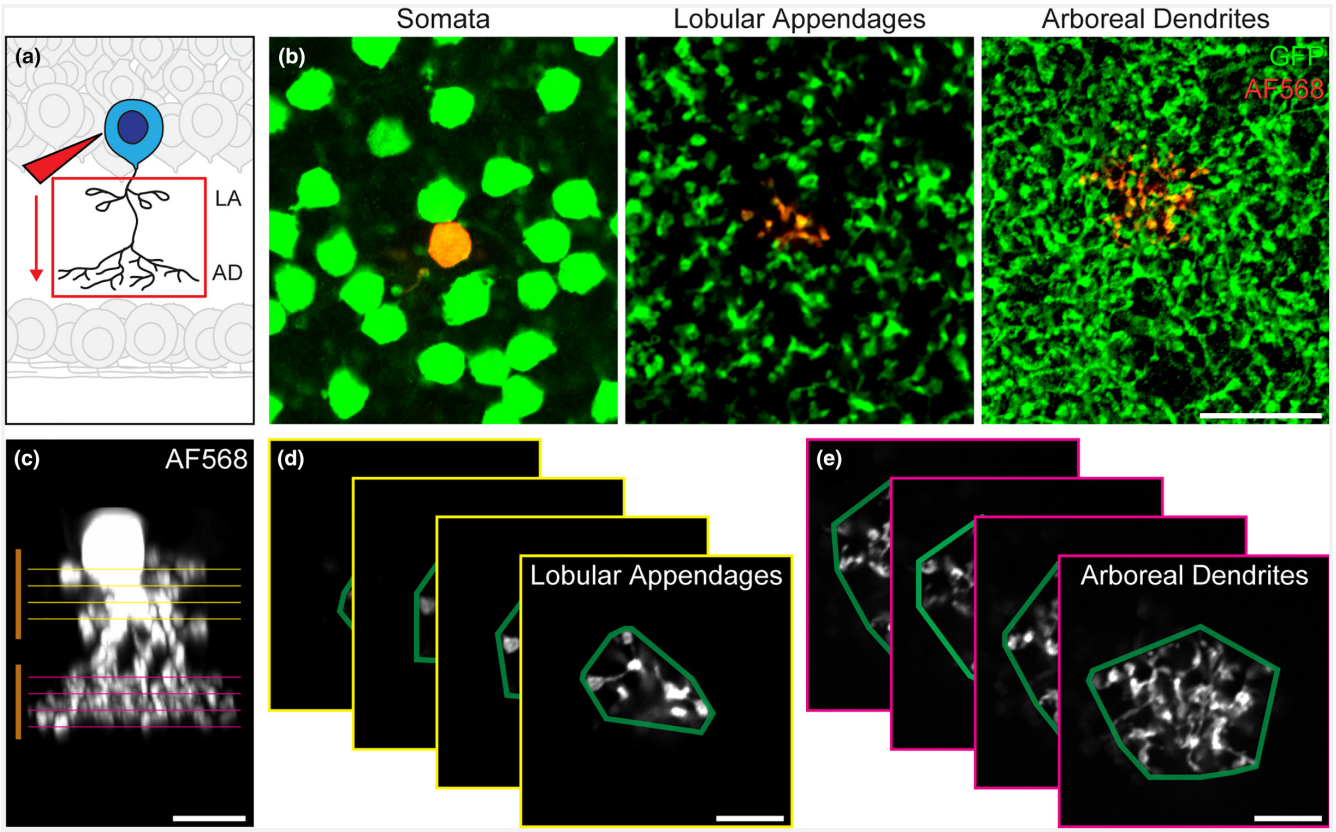


**FIGURE 8** Both the arboreal dendrites and the lobular appendages of AII amacrine cells can be labeled by injecting their somata (a), identified in *Cdh1-GFP* retinas, with AlexaFluor568 (b). Labeled AII amacrine cells can be assessed morphometrically for the depth of the inner plexiform layer occupied by the lobular appendages and arboreal dendrites (c) and for the respective areas of those fields, either in single planes or averaged across all depths through each arbor (d, e). Calibration bar = 25 μm in (b); 10 μm in (c–e)

field area, confirming that it increases for cells in the *Bax* KO retina (Figure 9e). This distinct behavior of the arboreal dendrites from the lobular appendages may be tied to their distinct functions: in particular, neighboring AII amacrine cells communicate directly to one another only through the former set of processes, via gap junctional contacts between their overlapping dendritic arbors. Perhaps this distinction necessitates differing growth strategies for each compartment of the AII amacrine cell.

But do the arboreal dendrites of these cells develop completely unresponsive to the density of homotypic neighbors? The *Cdh1-GFP*-labeled plexus for both sets of processes has expanded across a thicker IPL in the *Bax* KO retina (Figure 9f,g), as have the individual lobular terminal fields and arboreal dendritic fields measured from the injected cells (Figure 9h,i). At any depth through the arboreal dendritic arbor, however, the labeled dendritic skeleton within a single optical section (specifically, the single section where the arboreal dendritic arbor had the largest area defined by a convex polygon enclosing it; Figure 8e) showed a sparser dendritic arbor in the *Bax* KO retina (Figure 10a,b), confirmed by measuring the area of the skeleton itself (Figure 10c). That sparser arbor would suggest a reduction in branching density in response to the increase in dendritic overlap, a conclusion further supported by computing the percentage of the arbor's areal field occupied by the area of the dendritic skeleton; this too showed a significant reduction (Figure 10d). The former measure, the area of the dendritic skeleton itself (Figure 10c), also exhibited a moderately negative correlation with AII amacrine cell density (Figure 10e).

Despite such sparser dendritic branching, the entire dendritic skeleton (i.e. the sum of the skeletal areas in all optical sections containing it) was not significantly different from the littermate control retinas (Figure 10f), as it spanned a larger depth in the *Bax* KO retinas (Figure 9i). While one might consider the possibility that such a comparable total arboreal dendritic skeleton, between the two conditions, would suggest an intrinsic control upon its size, it is critical to keep in mind the large variability in the total volume of these skeletal arbors between individual cells. That variability is largely independent of local AII amacrine cell density (Figure 10g), unlike the *mean* skeletal arbor in a section (averaged across all sections of each cell) (Figure 10h), where skeletal branching is again found to be negatively correlated to AII amacrine cell density, even moreso than for the single sections containing the widest extent of the arboreal dendrites analyzed in Figure 10e. It is, consequently, difficult to envision an intrinsic specification of the volumetric skeletal size of the arboreal dendritic arbor when it varies so widely; rather, the present results suggest that the arboreal dendrites modulate one another's branching frequency to yield comparable local volumetric densities of their collective processes.

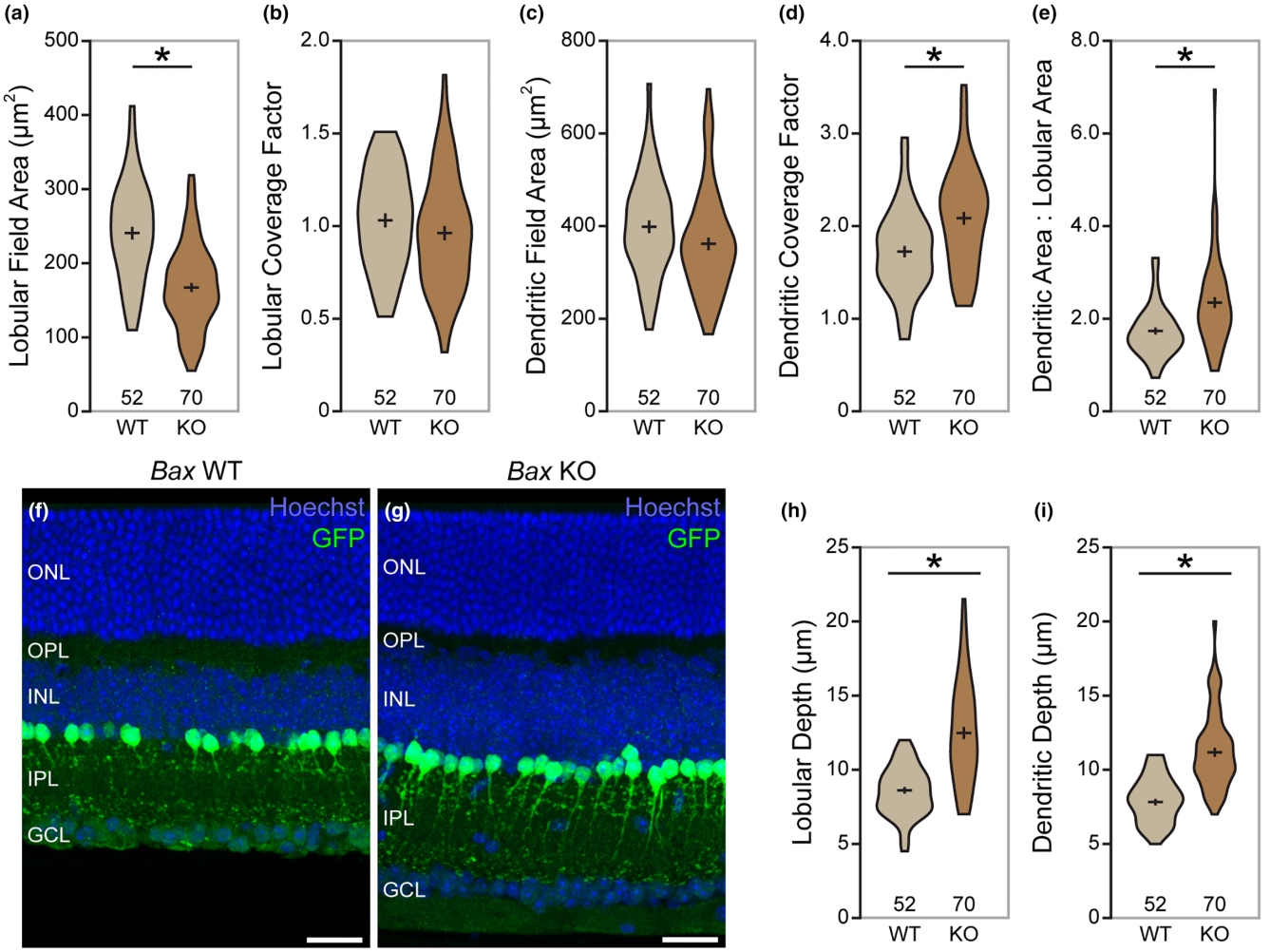


**FIGURE 9** AII amacrine cell number is significantly greater in the *Bax* KO, being increased by nearly 33%. As a consequence, the lobular terminal area is reduced (a; $p < 0.001$), achieving conservation of the calculated coverage factor, close to 1.0 (b; $p = 0.179$). Arboreal dendritic area is barely different in the *Bax* KO retina (c; $p = 0.079$), so that the calculated coverage factor is significantly increased for cells in the *Bax* KO retina (d; $p < 0.001$). The average number of rod bipolar cell axon terminals falling within the field of arboreal dendrites must therefore increase, as does the ratio of dendritic field area to lobular field area per cell (e; $p < 0.001$). Both the lobular appendages and arboreal dendrites expand across the depth of the retina in the *Bax* KO, evidenced in sections from the *Cdh1-GFP* retina (f, g). Measurements from the injected cells confirm this expansion of each compartment in the thicker inner plexiform layer of the *Bax* KO retina (h, i; $p < 0.001$ for both). Calibration bar = 25 μm in (f) and (g). *n* = the number of cells analyzed in each group; *indicates statistically significant result

The negative correlation between arboreal skeletal area and AII amacrine cell density (Figure 10e,h) would suggest that the variable sizes of those dendritic skeleta bear some direct relationship to one another, yielding a local variability in the extent to which neighboring dendritic arbors intersect. If homotypic cells modulate their branching density in the presence of excess dendritic arbors to maintain a constant volumetric presence of AII dendritic branches, then the volumetric density of their gap junctions should be conserved in the *Bax* KO retina. Like the radial expansion of the arboreal dendritic plexus, so the distribution of Connexin 36 (CX36) labeling, being the gap junctional protein linking AII amacrine cells (Feigenspan et al., 2001; Mills et al., 2001), is similarly expanded in the radial dimension. Single optical sections labeled for CX36 in wholemount preparations show that, within any 1-μm thick volume, density appears to be conserved (compare top panels in Figure 11a with 11b). Because the skeleta in any optical section are smaller in the *Bax* KO retina, so the number of CX36 puncta associated with those skeleta should be reduced (compare bottom panels in Figure 11a with 11b). But because of the expansion of the arboreal dendritic arbor across depth, the total number of CX36 puncta per cell did not differ between the two conditions (Figure 11c), despite the 34% increase in AII amacrine cells in the *Bax* KO retina. The total number of CX36 puncta per cell was robustly correlated to the total dendritic skeletal volume (Figure 11d). Computing the number of CX36 puncta per average skeletal area in a section, for each cell, and then multiplying by the density of AII amacrine cells within the field, yields a comparable spatial density between the two groups (Figure 11e), as suggested by the images of CX36 labeling in single optical sections (Figure 11a,b). It is, as above, difficult to envision how such a uniformity in the distribution of gap junctional contacts in the presence

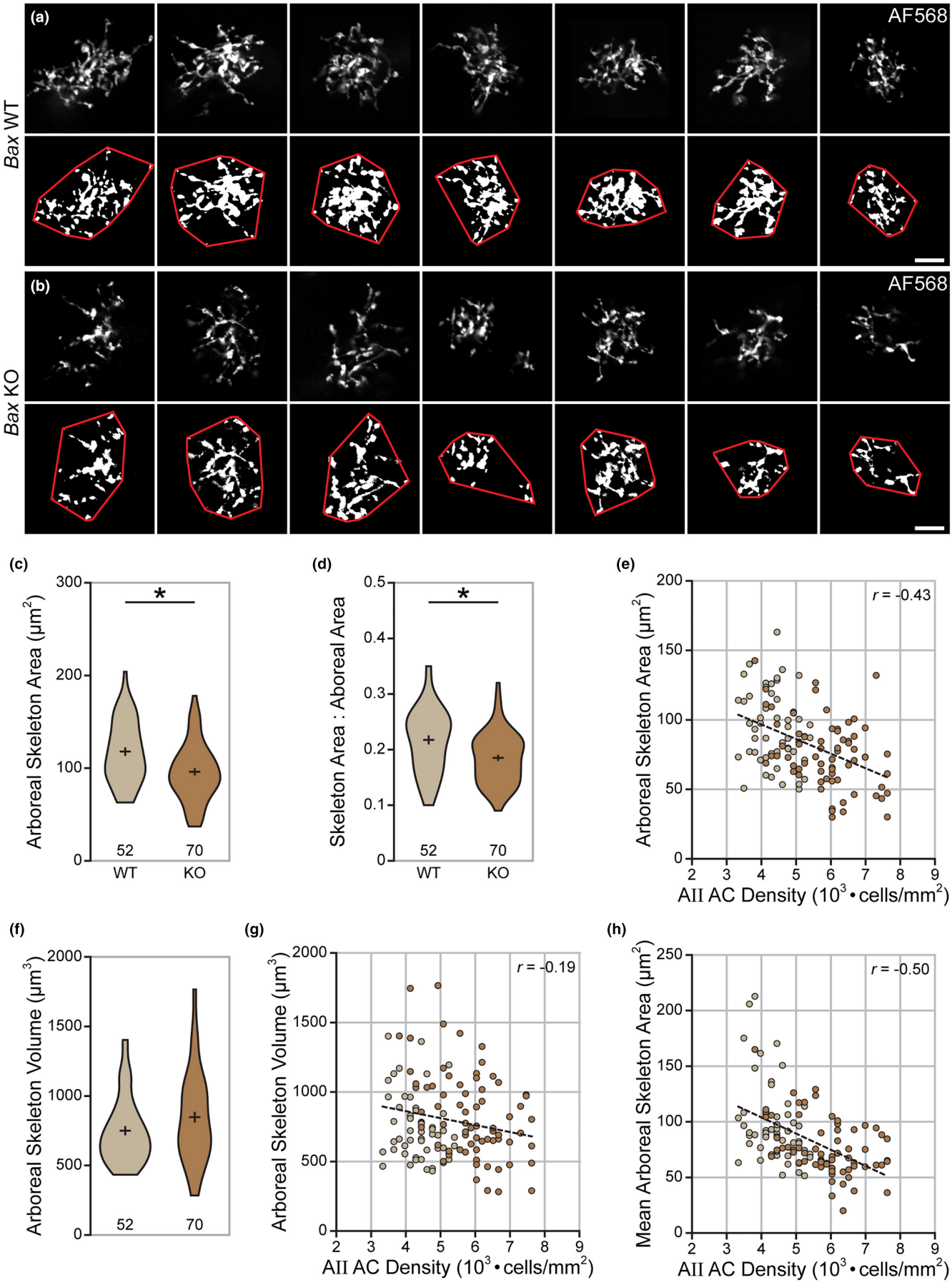

**FIGURE 10** Single optical sections through the inner parts of the IPL from seven different AII amacrine cells from each condition show that the branching density of single AII arboreal dendrites (the dendritic skeleton, in a single optical section) is reduced in the *Bax* KO retina (a, b). By measuring the area of this skeleton in the single optical section where its areal domain (defined by a convex polygon enclosing it) is largest, this measure of branching density is significantly lower in the *Bax* KO retina (c; $p < 0.001$), as is the ratio of this measure to the area of that convex polygon enclosing it (d; $p < 0.001$). Note that these skeletal areas are negatively correlated to the local density of AII amacrine cells (e). While there is a decrease in branching density at any depth within the arboreal dendritic arbor, the increase in the depth of the arbor across the thicker inner plexiform layer yields a total dendritic skeletal volume that is not significantly different (f; $p = 0.068$). That total sketetal volume is conspicuously variable across both populations (*Bax* WT and KO cells) and shows no relationship to the local density of AII amacrine cells (g). If that total skeletal volume is divided by the depth of the arbor (i.e. the sum of the number of optical sections containing it), to yield the mean skeletal area per cell in a section, this measure is even more negatively correlated to the variation in AII amacrine cell density (h). Calibration bar = 10 μm in (a, b). *n* = the number of cells analyzed in each group; *indicates statistically significant result

of a 34% increase in the population of AII amacrine cells can be generated without these cells interacting homotypically (Figure 11f).

## 4 | DISCUSSION

In the absence of genetic variance, the specification of cell number is acutely precise. When genetic variants that modulate complex traits are free to circulate within a population, however, cell number can vary considerably between members of the same species. For instance, by crossing two inbred strains of mice, each with low within-strain variability in total RGC number, and then generating a heterozygous F2 generation by mating those isogenic F1 offspring, inter-individual variability in RGC number amongst those F2 mice far exceeds that for either parental or F1 strains (Williams et al., 1998). As a consequence, those individual F2 mice, and other genetically heterogeneous populations like us, benefit from plasticity in the formation of connectivity between afferent and target neurons described here. Doubtless, each cell type differentiates its type-specific morphology through unique genetic specification driving that differentiation, and there may be intrinsic upper limits upon maximal field size, dendritic endings, and synaptic contacts. But the rules governing the developmental plasticity described herein ensure uniform process coverage while sampling from the entirety of afferents across the retina, regardless of variation in density across retinal eccentricity. As the AII amacrine cell population has a somal distribution that is indistinguishable from a random distribution of similarly sized cells, this would further necessitate a role for homotypic interactions, rather than a purely intrinsic specification, to yield any uniformity in their functional contribution across the retina (Keeley & Reese, 2018). While it is true that the numbers of other cell types are also altered in the *Bax* KO retina, it is difficult to appeal to either an afferent or target specification of either rod bipolar or AII amacrine morphology that can account for the scaling behavior of their processes or for the uniformity in the distribution of CX36 gap junctions.

The plasticity conserving a constant coverage factor appears to be the rule, for all of the dendritic populations within the OPL (but see Reese, 2018; Soto et al., 2013, 2018, for a consideration of the horizontal cell's axon terminal system in the OPL). Within the IPL, there appears to be no universal rule, as RGC populations appear to either tile or to modulate their overlying dendritic arbors to preserve uniform process density (Bae et al., 2018; Dacey, 1993; but see Lin et al., 2004). Amongst amacrine cell populations, the cholinergic amacrine cells do not alter their field extent or branching density when homotypic density varies across strains or through experimental manipulations (Farajian et al., 2004; Keeley et al., 2007), while dopaminergic amacrine cells do not preserve their plexus density in the presence of large variation in their numbers (Sankaran et al., 2018). VGluT3 amacrine cells behave like the overlapping dendritic appendages of AII amacrine cells, modulating process branching in proportion to a three-fold increase in dendritic coverage factor in the *Bax* KO retina (Keeley et al., 2021). What distinguishes the AII amacrine cell, amongst those other amacrine cell types, is that it differentiates two different sets of processes, each arising at distinct developmental stages (Gamlin et al., 2020) and that behave independently when homotypic densities vary. That latter independence suggests that AII cells must traffic unique proteins to the lobular versus dendritic compartments enabling the former to prohibit overlap while allowing the latter to intermingle and in turn interact, modulating branching density to ensure comparable volumetric coverage.

It should be apparent, then, in the presence of such plasticity accommodating the independent control of afferent versus target cell densities, that the synaptic convergence or divergence between pre- and post-synaptic cells will itself vary accordingly, so that the absolute number of synaptically connected cells to any given cell, as well as the number of synapses shared between individual pre- and post-synaptic cells, are also not species-specific traits. The lobular appendages tile, and the size of those tiling lobular fields vary as a function of homotypic density, which across the RI strains can increase by over 50% (Figure 3c). Within those lobular fields across the strains, their favored bipolar target is the type 2 cone bipolar cell (Graydon et al., 2018; Tsukamoto & Omi, 2017), a cell type that also varies by a comparably large magnitude across the strains (45%), but where that variation is not significantly correlated to the variation in AII amacrine cell number nor to the variation in other OFF cone bipolar cell populations (Keeley et al., 2014). Consequently, the absolute number of type 2 cone bipolar cells contacted will vary, as will the proportion of bipolar-directed output synapses made by an AII amacrine cell directed onto a single type 2 cell. At the population level, however, given that the axonal arbors of all bipolar cell types are expected to tile, the proportion of bipolar-directed output synapses onto the type 2 cone bipolar cell population may prove to remain constant.

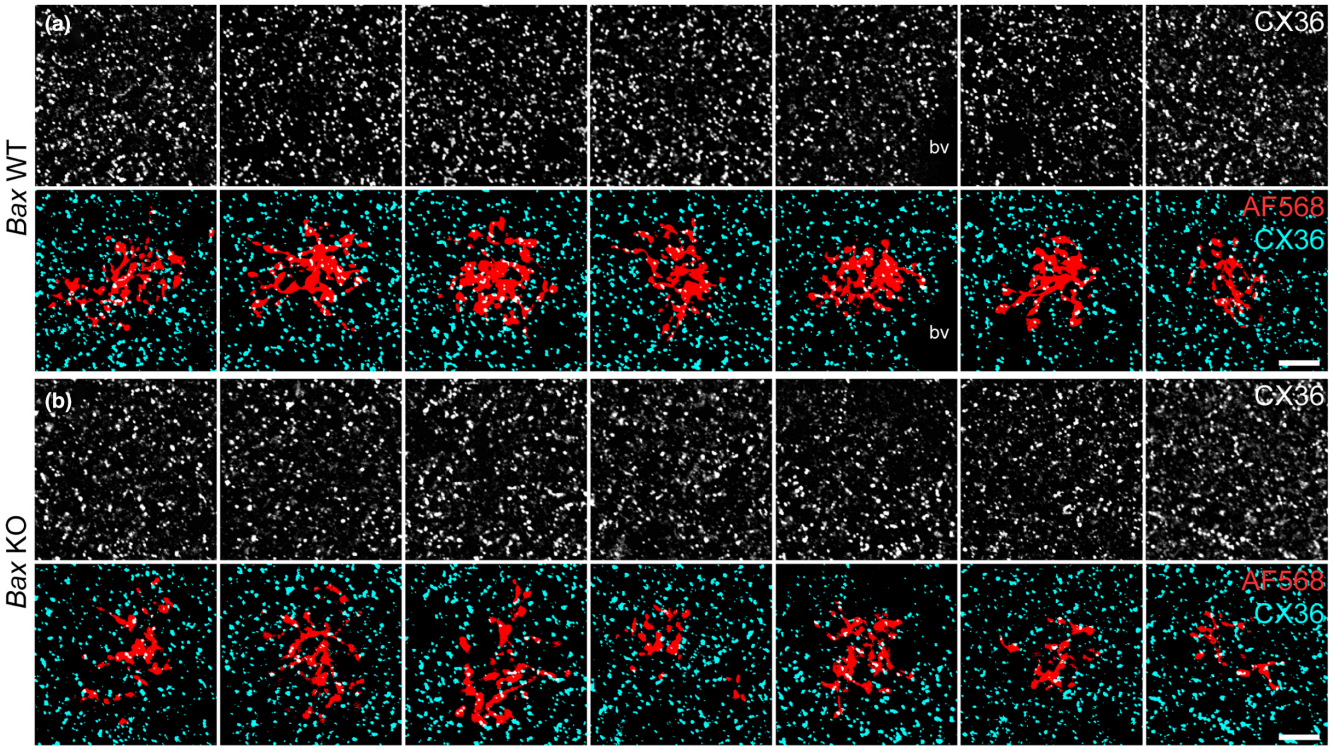


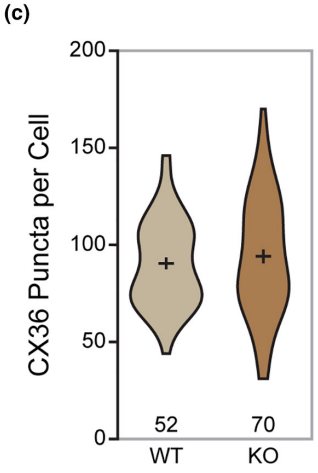


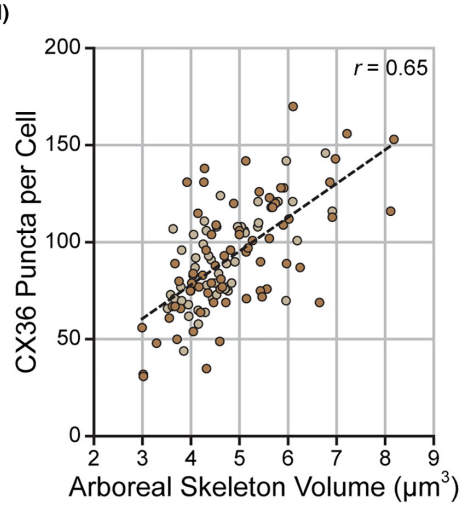


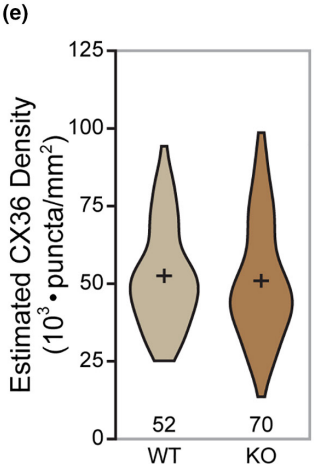


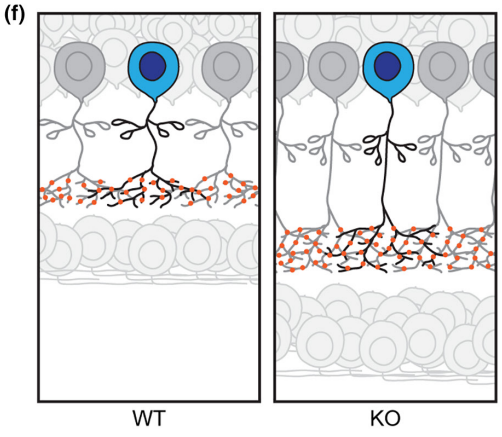

**FIGURE 11** Single optical sections through the inner portion of the IPL in wholemount preparations labeled for connexin 36 (CX36) show that, despite the increase in the density of AII amacrine cells, the density of CX36 puncta in the *Bax* KO retina appears comparable to controls (a, b; compare top panels). CX36 labeling in each optical section can be associated with the dendritic skeleton for each cell (shown here for the same seven cells; a, b; bottom panels). The total number of CX36 puncta per entire arboreal dendritic skeleton is comparable in *Bax* KO and WT cells (c; $p = 0.469$), being correlated to the overall size of the total arboreal dendritic skeleton (d). Dividing the number of puncta per cell by the depth of the arboreal dendritic arbor, and then multiplying by the density of AII cells within the field, one achieves a calculated mean spatial density of puncta (at any depth) that is comparable between the two conditions (e; $p = 0.625$), as suggested by those single optical sections themselves (top panels in a, b). AII amacrine cells, therefore, modulate the areal spread of their lobular terminal arbors according to local homotypic density to achieve a tiling of the OFF stratum in the inner plexiform layer, while their arboreal dendritic arbors instead reduce their local branching density in proportion to local AII cell density. This reduced branch density per cell, in response to heightened cell densities, ensures a conserved density of CX36 gap junctions (f). bv = indicates the presence of a blood vessel disrupting the CX36 distribution. Calibration bar = 10 μm in (a) and (b). *n* = the number of cells analyzed in each group

Of course, the size of an axonal or dendritic arbor does not necessarily imply identical connectivity within it. For instance, each cone pedicle is colonized by a single type 7 cone bipolar cell (Lee et al., 2011), although pedicles at the boundary of neighboring dendritic fields may be contacted by both arbors, where the number of terminal endings at the pedicle for each bipolar cell is reduced due to their shared colonization (Keeley & Reese, 2010; Wässle et al., 2009). This arrangement is even more pronounced for the horizontal cells, where each pedicle must form contacts with roughly six overlapping dendritic arbors. There, the number of contacts formed at a pedicle with each dendritic arbor is inversely related to the distance of the pedicle from the horizontal cell itself, implying that the total number of dendritic endings from those six horizontal cells should be conserved per pedicle. Interestingly, this relationship emerges during postnatal development from an initially more uniform colonization of all pedicles within each horizontal cell's dendritic field (Reese et al., 2005), a reorganization of the dendritic field that is independent of visual activity (Raven et al., 2008). And single rod bipolar axonal arbors contact multiple AII amacrine cells, yet they distribute the majority of their contacts to just one of the latter cells (Strettoi et al., 1992; Tsukamoto & Omi, 2013). What determines this preferential connectivity, and whether it emerges during development from an initially more even distribution remains to be determined.

## AUTHOR CONTRIBUTIONS

P.W.K. and B.E.R. designed the experiments; P.W.K. performed the experiments and collected the data; S.S.P. conducted the data analysis; P.W.K. and B.E.R. interpreted the data; P.W.K. and B.E.R. wrote the manuscript.

## DATA AVAILABILITY STATEMENT

The data that support the findings of this study are available from the corresponding author upon reasonable request.

## ORCID

*Patrick W. Keeley* https://orcid.org/0000-0003-1260-498X

## REFERENCES

Anastassov, I.A., Wang, W.W. & Dunn, F.A. (2019) Synaptogenesis and synaptic protein localization in the postnatal development of rod bipolar cell dendrites in mouse retina. *Journal of Comparative Neurology*, 527, 52–66.

Bae, J.A., Mu, S., Kim, J.S., Turner, N.L., Tartavull, I., Kemnitz, N. et al. (2018) Digital museum of retinal ganglion cells with dense anatomy and physiology. *Cell*, 173, 1293–1306.

Bleckert, A., Schwartz, G.W., Turner, M.H., Rieke, F. & Wong, R.O. (2014) Visual space is represented by nonmatching topographies of distinct mouse retinal ganglion cell types. *Current Biology*, 24, 310–315.

Buss, R.R., Sun, W. & Oppenheim, R.W. (2006) Adaptive roles of programmed cell death during nervous system development. *Annual Review of Neuroscience*, 29, 1–35.

Camerino, M.J., Engerbretson, I.J., Fife, P.A., Reynolds, N.B., Berria, M.H., Doyle, J.R. et al. (2021) OFF bipolar cell density varies by subtype, eccentricity, and along the dorsal ventral axis in the mouse retina. *Journal of Comparative Neurology*, 529, 1911–1925.

Carter-Dawson, L.D. & LaVail, M.M. (1979) Rods and cones in the mouse retina. I. Structural analysis using light and electron microscopy. *Journal of Comparative Neurology*, 188, 245–262.

Cepko, C.L., Austin, C.P., Yang, X., Alexiades, M. & Ezzeddine, D. (1996) Cell fate determination in the vertebrate retina. *Proceedings of the National Academy of Sciences of the United States of America*, 93, 589–595.

Dacey, D.M. (1993) The mosaic of midget ganglion cells in the human retina. *The Journal of Neuroscience*, 13, 5334–5355.

Demb, J.B. & Singer, J.H. (2012) Intrinsic properties and functional circuitry of the AII amacrine cell. *Visual Neuroscience*, 29, 51–60.

Edqvist, P.H., Lek, M., Boije, H., Lindbäck, S.M., and Hallböök, F. (2008) Axon-bearing and axon-less horizontal cell subtypes are generated consecutively during chick retinal development from progenitors that are sensitive to follistatin. *BMC Developmental Biology* 8:46, Available from: https://doi.org/10.1186/1471-1213X-1188-1146

Famiglietti, E.V. & Kolb, H. (1975) A bistratified amacrine cell and synaptic circuitry in the inner plexiform layer of the retina. *Brain Research*, 84, 293–300.

Farajian, R., Raven, M.A., Cusato, K. & Reese, B.E. (2004) Cellular positioning and dendritic field size of cholinergic amacrine cells are impervious to early ablation of neighboring cells in the mouse retina. *Visual Neuroscience*, 21, 13–22.

Feigenspan, A., Teubner, B., Willecke, K. & Weiler, R. (2001) Expression of neuronal connexin36 in AII amacrine cells of the mammalian retina. *The Journal of Neuroscience*, 21, 230–239.

Gamlin, C.R., Zhang, C., Dyer, M.A. & Wong, R.O.L. (2020) Distinct developmental mechanisms act independently to shape biased synaptic divergence from an inhibitory neuron. *Current Biology*, 30, 1258–1268.

Graydon, C.W., Lieberman, E.E., Rho, N., Briggman, K.L., Singer, J.H. & Diamond, J.S. (2018) Synaptic transfer between rod and cone pathways mediated by AII amacrine cells in the mouse retina. *Current Biology*, 28, 2739–2751.

Hughes, A.E., Enright, J.M., Myers, C.A., Shen, S.Q. & Corbo, J.C. (2017) Cell type-specific epigenomic analysis reveals a uniquely closed

chromatin architecture in mouse rod photoreceptors. *Scientific Reports*, 7, 43184.

Jeon, C.-J., Strettoi, E. & Masland, R.H. (1998) The major cell populations of the mouse retina. *The Journal of Neuroscience*, 18, 8936–8946.

Johnson, R.E., Tien, N.W., Shen, N., Pearson, J.T., Soto, F. & Kerschensteiner, D. (2017) Homeostatic plasticity shapes the visual system's first synapse. *Nature Communications*, 8, 1220.

Keane, T.M., Goodstadt, L., Danecek, P., White, M.A., Wong, K., Yalcin, B. et al. (2011) Mouse genomic variation and its effect on phenotypes and gene regulation. *Nature*, 477, 289–294.

Keeley, P.W., Lebo, M.C., Vieler, J.D., Kim, J.J., St John, A.J. & Reese, B.E. (2021) Interrelationships between cellular density, mosaic patterning, and dendritic coverage of VGluT3 amacrine cells. *The Journal of Neuroscience*, 41, 103–117.

Keeley, P.W., Luna, G., Fariss, R.N., Skyles, K.A., Madsen, N.R., Raven, M.A., Poché, R.A., Swindell, E.C., Jamrich, M., Oh, E.C., Swaroop, A., Fisher, S.K. & Reese, B.E. (2013) Development and plasticity of outer retinal circuitry following genetic removal of horizontal cells. *The Journal of Neuroscience*, 33, 17847–17862.

Keeley, P.W. & Reese, B.E. (2010) Role of afferents in the differentiation of bipolar cells in the mouse retina. *The Journal of Neuroscience*, 30, 1677–1685.

Keeley, P.W. & Reese, B.E. (2018) The somal patterning of the AII amacrine cell mosaic in the mouse retina is indistinguishable from random simulations matched for density and constrained by soma size. *Visual Neuroscience*, 35, e003.

Keeley, P.W., Whitney, I.E., Madsen, N.R., St. John, A.J., Borhanian, S., Leong, S.A. et al. (2014) Independent genomic control of neuronal number across retinal cell types. *Developmental Cell*, 30, 103–109.

Keeley, P.W., Whitney, I.E., Raven, M.A. & Reese, B.E. (2007) Dendritic spread and functional coverage of starburst amacrine cells. *Journal of Comparative Neurology*, 505, 539–546.

Keeley, P.W., Whitney, I.E. & Reese, B.E. (2017) Genomic control of retinal cell number: challenges, protocol, and results. In: Schughart, K. & Williams, R.W. (Eds.) *Methods in molecular biology: systems genetics*. New York: Springer, pp. 365–390.

Lee, S.C., Cowgill, E.J., Al-Nabulsi, A., Quinn, E.J., Evans, S.M. & Reese, B.E. (2011) Homotypic regulation of neuronal morphology and connectivity in the mouse retina. *The Journal of Neuroscience*, 31, 14126–14133.

Lin, B., Wang, S.W. & Masland, R.H. (2004) Retinal ganglion cell type, size, and spacing can be specified independent of homotypic dendritic contacts. *Neuron*, 43, 475–485.

Marc, R.E., Anderson, J.R., Jones, B.W., Sigulinsky, C.L. & Lauritzen, J.S. (2014) The AII amacrine cell connectome: a dense network hub. *Frontiers in Neural Circuits*, 8, 104. https://doi.org/10.3389/fncir.2014.00104

Mayordomo, R. (2001) Differentiated horizontal cells seem not to be affected by apoptosis during development of the chick retina. *International Journal of Developmental Biology*, 45, S79–S80.

Mills, S.L., O'Brien, J.J., Li, W., O'Brien, J. & Massey, S.C. (2001) Rod pathways in the mammalian retina use connexin 36. *Journal of Comparative Neurology*, 436, 336–350.

Nadal-Nicolas, F.M., Kunze, V.P., Ball, J.M., Peng, B.T., Krishnan, A., Zhou, G. et al. (2020) True S-cones are concentrated in the ventral mouse retina and wired for color detection in the upper visual field. *eLife*, 9, e56840.

Péquignot, M.O., Provost, A.C., Sallé, S., Taupin, P., Sainton, K.M., Marchant, D. et al. (2003) Major role of BAX in apoptosis during retinal development and in establishment of a functional postnatal retina. *Developmental Dynamics*, 228, 231–238.

Poché, R.A., Raven, M.A., Kwan, K.M., Furuta, Y., Behringer, R.R. & Reese, B.E. (2008) Somal positioning and dendritic growth of horizontal cells are regulated by interactions with homotypic neighbors. *European Journal of Neuroscience*, 27, 1607–1614.

Raven, M.A., Orton, N.C., Nassar, H., Williams, G.A., Stell, W.K., Jacobs, G.H., Bech-Hansen, N.T. & Reese, B.E. (2008) Early afferent signaling in the outer plexiform layer regulates development of horizontal cell morphology. *Journal of Comparative Neurology*, 506, 745–758.

Raven, M.A., Stagg, S.B., Nassar, H. & Reese, B.E. (2005) Developmental improvement in the regularity and packing of mouse horizontal cells: implications for mechanisms underlying mosaic pattern formation. *Visual Neuroscience*, 22, 569–573.

Reese, B.E. (2018) Axon terminal arbors of retinal horizontal cells lose control. *Frontiers in Neural Circuits*, 12, 82.

Reese, B.E. & Keeley, P.W. (2016) Genomic control of neuronal demographics in the retina. *Progress in Retinal and Eye Research*, 55, 246–259.

Reese, B.E., Keeley, P.W., Lee, S.C. & Whitney, I.E. (2011) Developmental plasticity of dendritic morphology and the establishment of coverage and connectivity in the outer retina. *Developmental Neurobiology*, 71, 1273–1285.

Reese, B.E., Raven, M.A. & Stagg, S.B. (2005) Afferents and homotypic neighbors regulate horizontal cell morphology, connectivity and retinal coverage. *The Journal of Neuroscience*, 25, 2167–2175.

Sankaran, M., Keeley, P.W., He, L., Iuvone, P.M. & Reese, B.E. (2018) Dopaminergic amacrine cell number, plexus density, and dopamine content in the mouse retina: strain differences and effects of Bax gene disruption. *Experimental Eye Research*, 177, 208–212.

Simmons, A.B., Camerino, M.J., Clemons, M.R., Sukeena, J.M., Bloomsburg, S., Borghuis, B.G. et al. (2019) Increased density and age-related sharing of synapses at the cone to OFF bipolar cell synapse in the mouse retina. *Journal of Comparative Neurology*, 528, 1140–1156.

Soto, F., Watkins, K.L., Johnson, R.E., Schottler, F. & Kerschensteiner, D. (2013) NGL-2 regulates pathway-specific neurite growth and lamination, synapse formation, and signal transmission in the retina. *The Journal of Neuroscience*, 33, 11949–11959.

Soto, F., Zhao, L. & Kerschensteiner, D. (2018) Synapse maintenance and restoration in the retina by NGL2. *eLife*, 7, e30388.

Strettoi, E., Raviola, E. & Dacheux, R.F. (1992) Synaptic connections of the narrow-field, bistratified rod amacrine cell (AII) in the rabbit retina. *Journal of Comparative Neurology*, 325, 152–168.

Szmajda, B.A., Grünert, U. & Martin, P.R. (2005) Mosaic properties of midget and parasol ganglion cells in the marmoset retina. *Visual Neuroscience*, 22, 395–404.

Tsukamoto, Y. & Omi, N. (2013) Functional allocation of synaptic contacts in microcircuits from rods via rod bipolar to AII amacrine cells in the mouse retina. *Journal of Comparative Neurology*, 521, 3541–3555.

Tsukamoto, Y. & Omi, N. (2017) Classification of mouse retinal bipolar cells: type-specific connectivity with special reference to rod-driven AII amacrine pathways. *Frontiers in Neuroanatomy*, 11, 92.

Vaney, D.I. (1985) The morphology and topographic distribution of AII amacrine cells in the cat retina. *Proceedings of the Royal Society, London*, 224, 475–488.

Vaney, D.I., Gynther, I.C. & Young, H.M. (1991) Rod-signal interneurons in the rabbit retina: 2. AII amacrine cells. *Journal of Comparative Neurology*, 310, 154–169.

Wässle, H., Puller, C., Müller, F. & Haverkamp, S. (2009) Cone contacts, mosaics and territories of bipolar cells in the mouse retina. *The Journal of Neuroscience*, 29, 106–117.

Whitney, I.E., Raven, M.A., Ciobanu, D.C., Poché, R.A., Ding, Q., Elshatory, Y. et al. (2011) Genetic modulation of horizontal cell number in the mouse retina. *Proceedings of the National Academy of Sciences of the United States of America*, 108, 9697–9702.

Whitney, I.E., Raven, M.A., Lu, L., Williams, R.W. & Reese, B.E. (2011) A QTL on chromosome 10 modulates cone photoreceptor number in the mouse retina. *Investigative Ophthalmology and Visual Science*, 52, 3228–3236.

Williams, R.W., Gu, J., Qi, S. & Lu, L. (2001) The genetic structure of recombinant inbred mice: high-resolution consensus maps for

complex trait analysis. *Genome Biology*, 2, RESEARCH0046. https://doi.org/10.1186/gb-2001-2-11-research0046

Williams, R.W., Strom, R.C., Zhou, G. & Yan, Z. (1998) Genetic dissection of retinal development. *Seminars in Cell & Developmental Biology*, 9, 249–255.

Yalcin, B., Wong, K., Agam, A., Goodson, M., Keane, T.M., Gan, X.C. et al. (2011) Sequence-based characterization of structural variation in the mouse genome. *Nature*, 477, 326–329.

Young, H.M. & Vaney, D.I. (1991) Rod-signal interneurons in the rabbit retina: 1. Rod bipolar cells. *Journal of Comparative Neurology*, 310, 139–153.

**How to cite this article:** Keeley, P.W., Patel, S.S. & Reese, B.E. (2022) Cell numbers, cell ratios, and developmental plasticity in the rod pathway of the mouse retina. *Journal of Anatomy*, 00, 1–19. Available from: https://doi.org/10.1111/joa.13653